CHALMERS

Simulations of high intensity laser-plasma interactions

Generating radiation of extreme intensity

GUSTAV MÅRTENSSON

Master's Thesis in Applied Physics

Department of Applied Physics
Division of Condensed Matter Theory
CHALMERS UNIVERSITY OF TECHNOLOGY
Gothenburg, Sweden 2014

Master's Thesis 2014:XXX

Abstract

In this project the interaction between a dense plasma and a high-intensity laser pulse was studied through Particle-in-cell simulations. Nonlinear behavior in the plasma particle dynamics caused the ultra-relativistic particles to generate radiation of intensities much greater than that of the incident radiation. The possibility to boost laser intensities with a factor $\sim 10^3$ could open up for the probing of nonlinear effects in vacuum.
To explain the results a theoretical model called the Relativistic Electronic Spring Model was extended slightly to explain the behavior of the plasma particles during the interaction with the high-intensity laser of arbitrary polarization.

Acknowledgements

The author wishes to thank Arkady Gonoskov and Prof. Mattias Marklund at the Dept. of Condensed Matter Theory at Chalmers University of Technology for their help and supervision of this project.

Gustav Mårtensson, San Francisco September 14 2015

Contents

1 Introduction

The interaction between plasma and high-intensity laser pulses is an exciting research area where modern state-of-the-art lasers are approaching the ability to produce laser intensities of 10^{23} W/cm^2. This is more intensity than if all the sunlight that hits the surface of the earth is focused onto the tip of a hair. Increasing these laser intensities could open up for the possibility of probing nonlinear effects in vacuum such as vacuum polarization and relativistic ion plasmas [1].

1.1 Background and objective

The Condensed Matter Theory group at Chalmers University of Technology recently demonstrated that the irradiation of a plasma surface can convert a p-polarized laser pulse from femto- to attosecond range and increase the intensity of the pulse significantly. This is due to relativistic effects in the motions of the plasma particles.

The purpose of this study was to develop code to simulate these high intensity laser-plasma interactions ($I \sim 10^{22}$ W/cm^2) for an incident pulse of arbitrary polarization to see if it is possible to obtain even greater amplification than in the case of a p-polarized pulse. To ensure that the simulation results were reliable, the development of a theoretical model of the particle dynamics was developed.

1.2 Comments regarding the project

Throughout this project Heaviside-Lorentz units have been used; both in the simulations and in the theoretical model. All equations and derivations in this thesis are therefor given in these units with the speed of light $c = 1$, elementary charge $e = 1$ and electron mass $m_e = 1$.

Plasma simulations can be very time consuming − even when performed in only one spatial dimension. Since arbitrary polarization yields endless parameter combinations that can be simulated, the large scale simulations were focused on linear and circular polarization of the incident laser pulse. Other, more arbitrarily polarized waves, were simulated mainly for the purpose to compare the results with those obtained from the theoretical model developed describing the interactions.

1.3 Disposition of thesis

The theory section of this report covers two main topics. First, information on high intensity laser-plasma interactions together with the derivation of a theoretical model called the *Relativistic Electron Spring model for an Incident Wave of*

Arbitrary Polarization (RES-AP) in Sec. 2.2.2. Secondly, general theory regarding *Particle-In-Cell* (PIC) simulations for relativistic plasma particles is covered in Sec. 2.3.

The Simulation section (Sec. 3) aims to describe more specific parts regarding the performed PIC simulations in this project and the different experimental setups simulated. The results from these simulations are presented and analyzed in Sec. 4 and 5 and are compared to the results expected from the RES-AP model.

2 Theory

In Sec. 2.1 a general introduction to plasma is given together with the derivation of a theoretical physical model (RES-AP) for the particle dynamics in relativistic laser-plasma interactions. Plasma physics are usually simulated using Particle-in-cell codes, and the code used in this project is described in Section 2.3.

2.1 Plasma

Solid, liquid, gas and plasma are the four fundamental states of matter. Extreme heating of a gas causes the molecules to ionize and allows for the electrons to move freely and separated from the ions which gives the particles a net charge $\neq 0$. A gas consisting of charged particles like this is called a *plasma*.

2.1.1 Physical equations

The equations governing the motions of plasma particles are the Lorentz force in Eq. (1)

$$\mathbf{F} = \frac{\mathrm{d}\mathbf{p}}{\mathrm{d}t} = q\left(\mathbf{E} + \mathbf{v} \times \mathbf{B}\right) \tag{1}$$

combined with Maxwell's equations (in Heaviside-Lorentz units) in vacuum:

$$\nabla \cdot \mathbf{B} = 0 \tag{2a}$$

$$\nabla \times \mathbf{E} = -\frac{1}{c}\frac{\partial \mathbf{B}}{\partial t} \tag{2b}$$

$$\nabla \cdot \mathbf{E} = \rho \tag{2c}$$

$$\nabla \times \mathbf{B} = \frac{1}{c}\frac{\partial \mathbf{E}}{\partial t} + \frac{1}{c}\mathbf{j} \tag{2d}$$

where $\mathbf{F}$ is the force acting on a particle with charge q in an electric field and magnetic field of strenghts $\mathbf{E}$ and $\mathbf{B}$ respectively [2]. Together with externally applied fields the charged particles in the plasma give rise to the electric and magnetic fields due to their charge and motion. This makes the description of plasma particles and their movements very complex, since each individual particle will affect all the other particles by a force depending on its relative position, charge and velocity.

In this project the intensities of the laser are so great that the interaction with the plasma will make the particles move at velocities very close to the speed of light c. Relativistic effects plays a key role in the laser-plasma interactions and it is necessary to introduce the Lorentz factor γ defined as

$$\gamma = \frac{1}{\sqrt{1 - v^2/c^2}} \tag{3}$$

where $\mathbf{v}$ is the velocity of the plasma particle.

2.2 Physical model of high intensity laser-plasma interactions

To justify the results from the PIC simulations a theoretical model describing the laser-plasma interaction in the simulations was necessary. One model describing the interaction between a uniform, high-density plasma and a p-polarized laser pulse at oblique incidence is called the *Relativistic Electronic Spring* (RES) model [3]. This model has been extended slightly in this project to include an arbitrary pulse polarization (RES-AP).

The experimental setup that is simulated is described further in Sec. 2.2.1 together with necessary transformation properties when shifting from a stationary laboratory frame R to a moving frame of reference R'. The RES-AP model is derived in Sec. 2.2.2.

Parameters linked to the incident laser are denoted with the subscript L whereas the subscript T is linked to the Lorentz transformation. Unprimed variables corresponds to the stationary reference frame and primed to the moving reference frame. The subscript 0 corresponds to the initiatal or unperturbed value of a parameter.

2.2.1 Oblique incidence

Consider a dense plasma in two dimensions with an incident laser pulse at an angle θ to the normal of the sharp plasma boundary. To avoid a computationally heavy 2D PIC simulation a change from a stationary reference frame R to a moving reference frame R' can be made to turn the simulation into a much simpler 1D problem [4]. A shift by $v_T = c\sin\theta$ in the y-direction makes the laser normally incident to the plasma boundary as shown in Fig. 1. In this frame all entities (such as field amplitudes and plasma density) are considered uniform in the y- and z-direction at any given position x.

The Lorentz transformations from the stationary frame R to the moving frame R' are given by

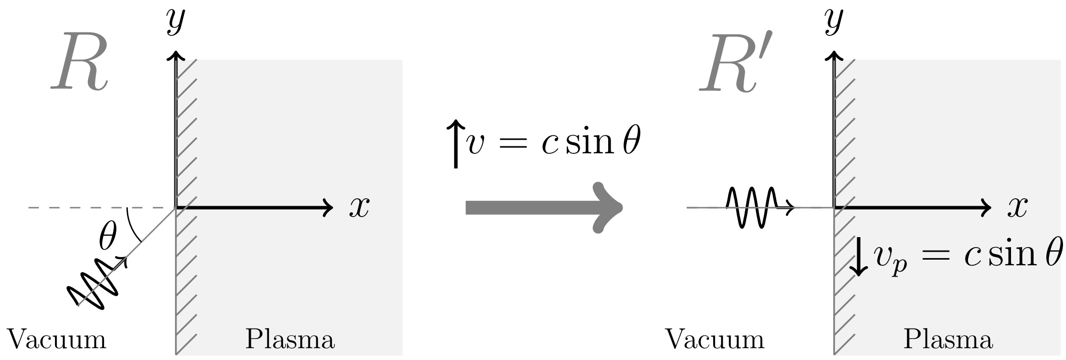

Figure 1: Illustration of the experimental setup as well as the transformation from the stationary reference frame R to the moving frame R'.

$$t' = \gamma_T(t - \beta_T \frac{y}{c}) \tag{4a}$$
$$x' = x \tag{4b}$$
$$y' = \gamma_T(y - \beta_T ct) \tag{4c}$$
$$z' = z \tag{4d}$$

with

$$\beta_T \equiv \frac{v_T}{c} = \sin\theta, \quad \gamma_T \equiv \frac{1}{\sqrt{1-\beta_T^2}} = \frac{1}{\cos\theta} \tag{5}$$

These transformation Doppler-shifts the wavelength of the incident laser as

$$\lambda' = \gamma_T \lambda = \lambda / \cos\theta \tag{6a}$$
$$\omega_L' = \omega_L / \gamma_T = \omega_L \cos\theta \tag{6b}$$

The electromagnetic fields of an arbitrarily polarized laser pulse transforms as

$$\mathbf{E} = \begin{pmatrix} -E_{y,0}\sin\theta \\ E_{y,0}\cos\theta \\ E_{z,0} \end{pmatrix} \rightarrow \mathbf{E}' = \begin{pmatrix} 0 \\ E_{y,0}\cos\theta \\ E_{z,0}\cos\theta \end{pmatrix} \tag{7a}$$

$$c\mathbf{B} = \begin{pmatrix} E_{y,0}\sin\theta \\ -E_{y,0}\cos\theta \\ E_{z,0} \end{pmatrix} \rightarrow c\mathbf{B}' = \begin{pmatrix} 0 \\ -E_{y,0}\cos\theta \\ E_{z,0}\cos\theta \end{pmatrix} \tag{7b}$$

where $E_{y,0}$ and $E_{z,0}$ are defined as the maximum field amplitude of the transverse waves oscillating in the x,y-plane and z-direction respectively in R. The field quantities are typically given in dimensionless units as

$$a_i = \tfrac{eE_i}{m_e \omega_L c} \quad , i = x,y,z \tag{8}$$

where $a_i \sim 1$ corresponds to ultra-relativistic particles. The Lorentz transformation will also affect the simulations due to contraction in the spatial y-direction by a factor γ_T^{-1}. This transforms the particle density as

$$n' = n \cos^{-1}\theta \tag{9}$$

If the plasma density n is greater than the critical density n_c the pulse will not be able to penetrate the plasma and will instead be reflected at the boundary. It is defined as

$$n_c = \omega_L^2 \frac{m_e \varepsilon_0}{e^2} \tag{10}$$

and hence depends on the laser frequency.

These transformations - and turning the 2D problem to a 1D problem - have been used in all simulations for this project. The RES-AP model is also developed for one spatial dimension in this moving reference frame R'.

2.2.2 Derivation of the Relativistic Electron Spring model for arbitrary polarization

The model derived is based on the *Relativistic Electron Spring* model developed in [3], which describes the dynamics of the boundary layer for a p-polarized laser interaction. This model was extended to describe the plasma interaction of a pulse with an arbitrary polarization and is called the RES-AP model.

The model describes the physical properties of the interaction in the moving reference frame R' and hence only depends on one spatial dimension. It is developed for dimensionless time t and position x according to

$$\begin{aligned} t &= \omega'_L \hat{t} \\ x &= \tfrac{\omega'_L}{c} \hat{x} \end{aligned} \tag{11}$$

which relates time and coordinate to the period time T'_L and wavelength λ'_L of the incident laser. The position x, time t and velocity $\beta_{x,y,z}$ are given in R' but the primes have been dropped in the derivation of the model for aesthetic reasons. The variable $a'_{L,z}(x,t)$ corresponds to the dimensionless field amplitude of the incident laser's z'-component at a given position x and time t in frame R', where $\max(a'_{L,z}(x,t=0) = a'_{z,0})$. Furthermore, a'_0 is defined as

$$a'_0 = \max\left(\sqrt{a'^2_{y,L}(x,t=0) + a'^2_{z,L}(x,t=0)}\right) \tag{12}$$

i.e. the maximum field amplitude in the y',z'-plane of the incident laser pulse. For a wave of linear polarization $a'_0 = a'_{y,0}$ and for circular polarization $a'_0 = a'_{y,0} = a'_{z,0}$.

The Relativistic Electron Spring model is based on three main assumptions about the system:

1. The plasma electrons are assumed to be part of one of two groups: one inside an infinitely narrow layer around a moving position x_s, where all electrons at position $x \in (0,x_s)$ have gathered, and one group for electrons at $x > x_s$ with an unperturbed plasma density n'_0.

2. All the electrons in the boundary layer have the same dimensionless velocity β_x, β_y and β_z. Since these electrons are ultra-relativistic it is assumed that $1 \approx \beta_x^2 + \beta_y^2 + \beta_z^2$ at all times.

3. The electrons in the boundary layer at $x \in (0, x_s)$ move collectively so that their motions generate radiation that compensates for the radiation of the incident pulse, i.e. the electrons move as if they were generating the radiation of the incident laser wave.

Assume a system in the moving frame R' with a laser pulse of arbitrary polarization (as described in the Eq. (7)), incident angle θ and unperturbed plasma density n'_0. When the pulse collides with the plasma the electrons close to the boundary will be pushed back due to the ponderomitive force. These electrons will accumulate and form a thin layer with its boundary at position $x_s(t)$ and an electron density much greater than the unperturbed density n'_0. This means that energy from the incident pulse is transferred and accumulated in this ultra-thin boundary layer [5]. When the electric field amplitude at x_s starts to decrease, the accumulated energy in the plasma causes the ultra-relativistic electrons to begin accelerate collectively towards the incidence pulse and in the process emit short bursts of high-intensity radiation with much shorter wavelength than that of the incident pulse. A sketch of the electron density at a boundary displacement of x_b ($x_b(t=0)=0$) is shown in Fig. 2 with the laser pulse moving in the positive x-direction.

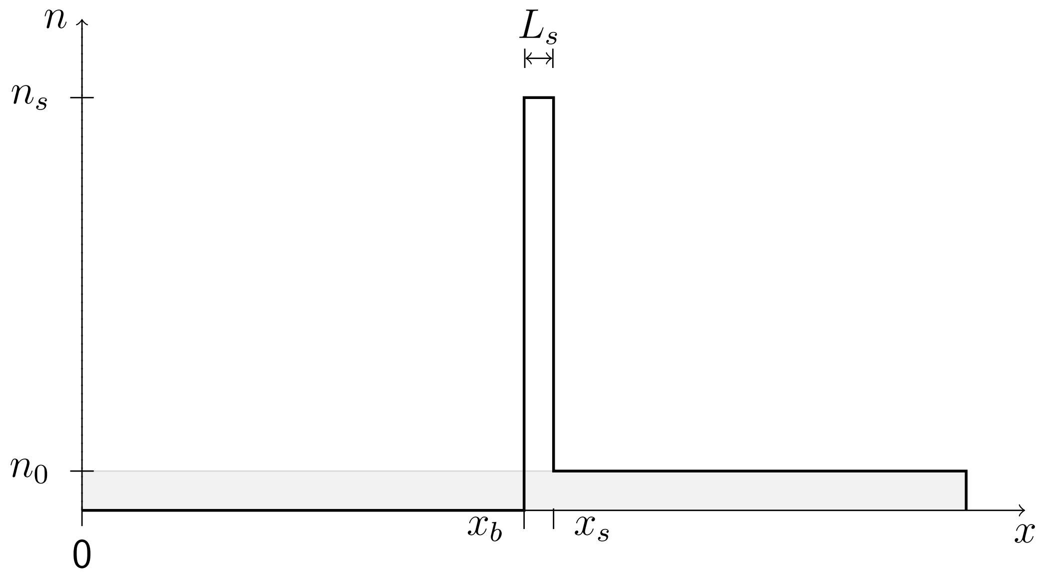

Figure 2: Sketch illustrating the electron density at the displacement $x_b(t)$ of the plasma boundary during laser interaction in accordance with the assumptions made for the RES-AP model. The gray area represent the ion density as well as the electron density before the laser collision. $L_s(t) = |x_b(t) - x_s(t)|$ and $n_s(t)$ are the thickness and electron density of the boundary layer at time t.

For an incident p-polarized polarized wave (i.e. $E'_{z,L} = B'_{y,L} = 0 \Leftrightarrow a'_{z,L} = 0$ at $t = 0$) this roughly means that the plasma electrons will accumulate energy in the electric field through charge separation by moving the plasma boundary x_b in the positive x-direction and increasing the electron density n' in a thin boundary layer. When the peak of the incident sinusoidal laser wave reaches the shifted plasma boundary at $x_b(t)$ the ultra-relativistic electrons move at a speed very close to c in the y-direction which consequently means that the $\beta_x \equiv \frac{v_x}{c} \approx \beta_z \approx 0$ since $\beta_x^2 + \beta_y^2 + \beta_z^2 < 1$. When the electric field starts to decrease at x_b the kinetic energy of the electrons will be shift from β_y to β_x so that $\beta_x \to -1$ and in this process emit radiation of short duration and extremely high intensity. This is described by the RES model and the shape of the radiation is dependent of both θ and S.

For an arbitrarily polarized wave $a'_{z,L}$ can be non-zero and have a phase shift of Ψ relative $a'_{y,L}$ which makes the particle dynamics a bit more complex. Assume a right-going circular polarization, i.e. $a'_{y,L}$ lagging $\Psi = \frac{\pi}{2}$ behind $a'_{z,L}$ and $a'_{y,0} = a'_{z,0} = a'_0$. When $a'_{z,L}(x_b,t) = 0$ at the plasma boundary x_b, $a'_{y,L}(x_b,t) = a'_0$ and the electron velocity $|\beta_y| \to 1$ which means that $\beta_x \not\to -1$. This counteracts the giant pulse generation, but means that more energy potentially can be transferred to the plasma boundary since not all energy is released in each wave cycle.

2.2.3 Dynamics of boundary electrons

The third of the three assumptions behind the model states that the perturbed electrons forming the boundary layer should compensate completely for the incident radiation. Putting up a coupled expression for this compensation the following equation obtained:

$$\frac{a'_{y,0}}{a'_0}\sin(t - x_s + \Psi)W_y(t,x_s,\Psi) = \frac{S}{2\cos^3\theta}\left(\sin\theta - \frac{\beta_y(t)}{1-\beta_x(t)}\right)x_s(t) \tag{13a}$$

$$\frac{a'_{z,0}}{a'_0}\sin(t - x_s)W_z(t,x_s,\Psi) = \frac{S}{2\cos^3\theta}\left(\frac{\beta_z(t)}{1-\beta_x(t)}\right)x_s(t) \tag{13b}$$

where Eq. (13a) and Eq. (13b) corresponds to the E'_y and E'_z fields respectively. The sine functions represents the field amplitude of the incident wave at time t and the position of the boundary layer's moving point $x_s(t)$. The functions W_y, W_z are window functions determining the length and shape of of the pulse components, and $S \equiv \frac{n_0}{n_c a_0}$ is the *similarity parameter* [6].

For a right-going circularly polarized wave the E'_y sinusoid initially has a phase shift of $\Psi = \frac{\pi}{2}$ relative the E'_z sinusoid. This is illustrated for a right-going circular polarized wave in Fig. 3 where the dashed lines corresponds to the window functions W_y, W_z.

The expression inside the parentheses in Eq. (13) corresponds to the radiation from the ions (with velocity $\sin\theta$ in the moving frame, $c = 1$) and the electrons in the boundary layer respectively. It can be shown [5, 7] that the radiation emitted from a moving layer with surface charge σ is, in Heaviside-Lorentz units, given by:

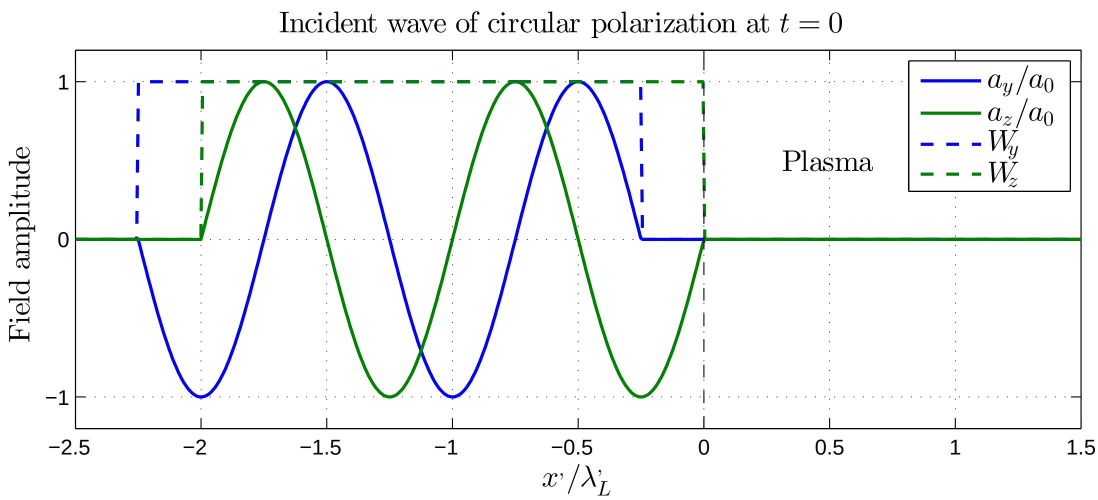

Figure 3: Illustration of how an incident left-going circularly polarized wave of two cycles length. The dashed lines represents the window functions described in Eq. (13) and the solid lines are the incident wave.

$$a_y^+(t) = \frac{\sigma}{2}\left(\frac{\beta_y(t)}{1-\beta_x(t)} - \sin\theta\right) \tag{14a}$$

$$a_y^-(t) = -\frac{\sigma}{2}\left(\frac{\beta_y(t)}{1+\beta_x(t)} - \sin\theta\right) \tag{14b}$$

$$a_z^+(t) = -\frac{\sigma}{2}\frac{\beta_z(t)}{(1+\beta_x(t))} \tag{14c}$$

$$a_z^-(t) = \frac{\sigma}{2}\frac{\beta_z(t)}{(1+\beta_x(t))} \tag{14d}$$

where a_y^+ (a_z^+) is the y-component (z-component) of the radiation emitted in the positive x-direction and a_y^- (a_z^-) in the negative direction. The surface charge layer constitutes of the electrons accumulated up to $x < x_s$ as stated in the first main assumption in the beginning of this section. This gives an expression of σ as

$$\sigma[x_s(t)] = \int_{-\infty}^{x_s(t)/\cos\theta} N(\chi)\mathrm{d}\chi \approx n_0\frac{x_s(t)}{\cos\theta}\Gamma = a_0\frac{n_0}{a_0\cos^2\theta}x_s(t) = a_0'\frac{S}{\cos^3\theta}x_s(t) \tag{15}$$

which together with Eq. (14a) are used for the expression for the wave compensation in Eq. (13).

The position $x_s(t)$ is coupled to the velocity according to

$$\frac{\mathrm{d}}{\mathrm{d}t}x_s(t) = \beta_x(t),\ x_s(t=0) = 0 \tag{16}$$

with the initial condition that an electron in the boundary layer is positioned at $x_s(t = 0) = 0$ at $t = 0$. The particles are assumed to be ultra-relativistic and the relation between the velocities can be written as

$$\gamma_p = \frac{1}{\sqrt{1 - (\beta_x^2 + \beta_y^2 + \beta_z^2)}} \tag{17}$$

where γ_p is the relativistic factor and becomes an additional parameter in the theoretical model. A specific values of γ_p can for instance be obtained through PIC-simulations with using the same values of S and θ.

Combining Eqs. (13), (16) and (17) a complete system of ordinary differential systems that describes the motion of an electron in the boundary layer is obtained. The radiation generated by the plasma boundary layer $a'_{y,g}$ and $a'_{z,g}$ at position $x_s(t)$ is then given by

$$a'_{y,g}[\xi(t)] = a'_0 \frac{S}{2\cos^3\theta} \left(\frac{\beta_y}{1+\beta_x} - \sin\theta \right) x_s(t) \tag{18a}$$

$$a'_{z,g}[\xi(t)] = -a'_0 \frac{S}{2\cos^3\theta} \frac{\beta_z}{(1+\beta_x)} x_s(t) \tag{18b}$$

where $\xi = x_s(t) + t$ is the *retarded time* which is convenient since the radiation is not emitted from the same position for all values of t but from the position $x_s(t)$.

Setting $a'_{z,0} = \Psi = 0$ corresponds to a p-polarized wave and turns the equations above into the original RES model.

2.3 The Particle-in-cell method

Simulating plasma particles requires the implementation of the Lorentz force in Eq. (1) and solving Maxwell's equations in Eq. (23) numerically for each single particle. For plasmas with densities between $n = 10^{22} - 10^{24}$ particles/cm^3 this would be incredibly computationally heavy or even impossible to compute, why it is necessary to simplify the numerical problem.

Plasma simulations is commonly performed by using the *Particle-In-Cell* (PIC) algorithm.

2.3.1 General outlines of the Particle-in-cell method

The basic idea of the PIC method is that letting so called *macroparticles* represent a large number of real plasma particles, and thus being able to significantly reduce the number of computational particles. This is possible since the Lorentz force (1) depends on the charge-to-mass ratio, which remains the same for the macroparticles.

The general principle of the algorithm is shown in Fig. 4 below.

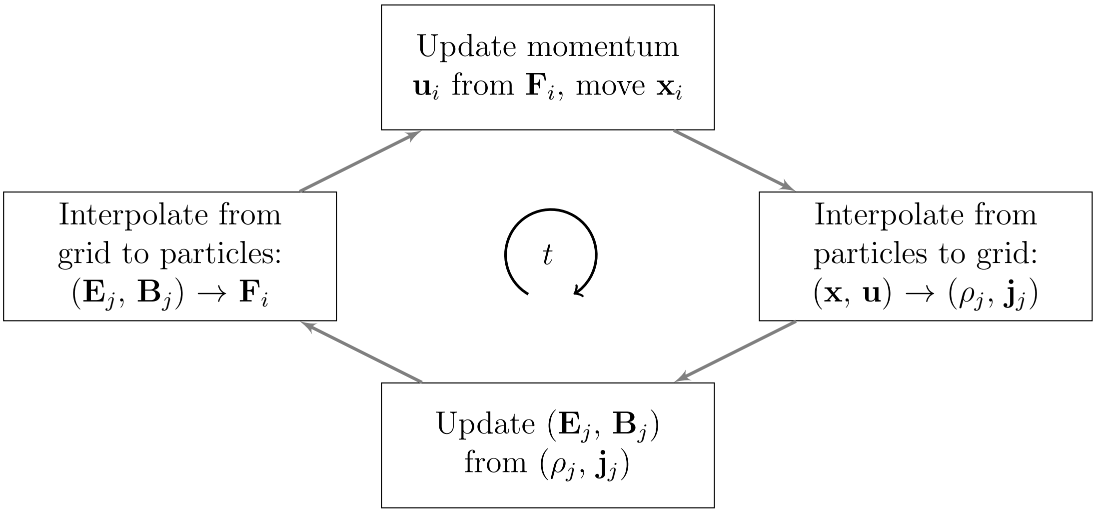

Figure 4: Flow chart of Particle-In-Cell algorithm.

Each macroparticle i has a position $\mathbf{x}_i$ and a momentum $\mathbf{u}_i$. These are used to compute the charge density ρ_j and current density $\mathbf{j}_j$ on every grid-point j at a mesh. Maxwell's equations (23) are solved on this grid, and from the obtained electric and magnetic field $\mathbf{E}$ and $\mathbf{B}$ the Lorentz force acting on each macroparticle is computed.

The Particle-in-cell algorithm hence contains two interpolation processes; one from the particle positions to the grid to compute the electromagnetic fields and one interpolation from the grid back to the particle's positions. This procedure can be done in different ways and is described in Section 2.3.2. The updating of the electromagnetic fields by solving Maxwell's equations is explained further in Section 2.3.4, and the rather tricky computation of the Lorentz force is described in Section 2.3.5.

2.3.2 Interpolation

The choice of interpolation scheme in the PIC algorithm from particle position to the mesh-grid is a trade-off between numerical accuracy and computational speed. The easiest method would be *Nearest Grid-Point* (NGP) interpolation, where the charge cloud would be assigned to the gridpoint closest to the corresponding particle. This method is very straightforward and easy to implement, but due to the simplicity of NGP it yields high levels of noise – especially if the number of macroparticles per cell is low.

A 1D example of a first-order weighting scheme is the *cloud-in-cell* (CIC) scheme and is shown in Fig. 5 with a mathematical description in Eq. (19).

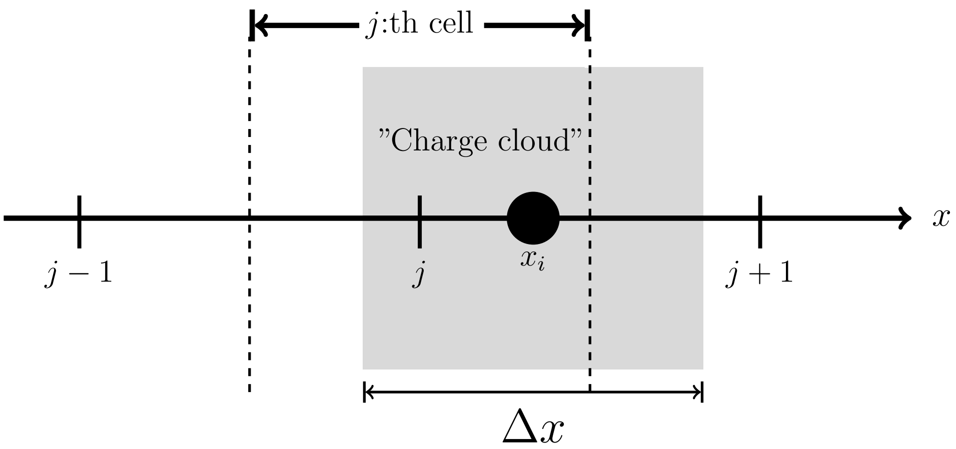

Figure 5: Sketch of the Cloud-in-cell interpolation scheme.

$$q_j = q_c \frac{X_{j+1} - x_i}{\Delta x} \tag{19a}$$

$$q_{j+1} = q_c \frac{x_i - X_j}{\Delta x} \tag{19b}$$

where q_c is the total cloud charge, X_j is the position of the j:th grid-point and the particle position $x_i \in [X_j, X_{j+1}]$.

When performing the second interpolation (i.e. when interpolating from the electromagnetic fields from the grid to the particles) there is a risk of a particle exerting a force on itself. However, if the same interpolation scheme is used this is avoided [8]. Hence, the grid-to-particle interpolation becomes

$$E(x_i) = E_j \frac{X_{j+1} - x_i}{\Delta x} + E_{j+1} \frac{x_i - X_j}{\Delta x} \tag{20}$$

where E_j is the electric field strength at grid-point j. The same equation holds for the magnetic field B.

The CIC scheme costs more computationally than NGP, but since noise is reduced the number of grid-points as well as macroparticles necessary to avoid non-physical effects in the PIC simulation are also reduced. It is possible to use quadratic or cubic splines as higher-order weighting which would further reduce the noise but again requires more computations. The CIC scheme has been used in the PIC simulations in this project.

2.3.3 Numerical methods

PIC simulations involves the solving of Maxwell's equations. There are number of different ways to solve PDE:s numerically such as *finite element method* (FEM) and *spectral method* which typically involves using Fast Fourier Transform. In this project the *finite difference method* was used.

Solving Maxwell's equations for an electrostatic problem (i.e. $\nabla \times \mathbf{E} = -\partial \mathbf{B}/\partial t \approx 0$) the equations to be solved are:

$$\begin{aligned} \mathbf{E} &= -\nabla \phi \\ \nabla \cdot \mathbf{E} &= \frac{\rho}{\epsilon_0} \end{aligned} \tag{21}$$

which are combined into *Poisson's equation*

$$\nabla^2 \phi = -\frac{\rho}{\epsilon_0} \tag{22}$$

For a one-dimensional problem in the x-direction, assume the charge density ρ_j is known at each grid-point j with equal grid-spacing Δx. The problem is discretized as a central-difference so that

$$E_x = -\frac{\partial \phi}{\partial x} \rightarrow E_{x,j} = -\frac{\phi_{j+1} - \phi_{j-1}}{2\Delta x} \tag{23a}$$

$$\frac{\partial^2 \phi}{\partial x^2} = -\frac{\rho}{\epsilon_0} \rightarrow \frac{\phi_{j-1} - 2\phi_j + \phi_{j-1}}{(\Delta x)^2} = -\frac{\rho_j}{\epsilon_0} \tag{23b}$$

for all j so that $j\Delta x \in [0,L]$ which is the computational domain. Known boundary conditions at $x = 0,\ L$ makes for equally many equations as unknowns and a solvable system.

2.3.4 Integration of field equations

The updating of the electric and magnetic field stance from the time derivatives of **E** and **B** in Maxwell's equations that are given by (in Heaviside-Lorentz units):

$$\frac{\partial \mathbf{B}}{\partial t} = -c\nabla \times \mathbf{E} \tag{24a}$$
$$\frac{\partial \mathbf{E}}{\partial t} = c\nabla \times \mathbf{B} - \mathbf{j} \tag{24b}$$

To update the fields a *leap-frog scheme* can be used. Assuming a 1D problem in the x-direction the equations in (24) is updated from time step t_n ($t_{n-\frac{1}{2}}$) to t_{n+1} ($t_{n+\frac{1}{2}}$) for the electric (magnetic) field according to

$$\frac{B^{n+\frac{1}{2}}_{z,j+\frac{1}{2}} - B^{n-\frac{1}{2}}_{z,j+\frac{1}{2}}}{\Delta t} = -c\frac{E^{n}_{y,j+1} - E^{n}_{y,j}}{\Delta x} \tag{25a}$$
$$\frac{E^{n+1}_{x,j+\frac{1}{2}} - E^{n}_{x,j+\frac{1}{2}}}{\Delta t} = -j^{n+\frac{1}{2}}_{x,j+\frac{1}{2}} \tag{25b}$$
$$\frac{E^{n+1}_{y,j} - E^{n}_{y,j}}{\Delta t} = -c\frac{B^{n+\frac{1}{2}}_{z,j+\frac{1}{2}} - B^{n+\frac{1}{2}}_{z,j-\frac{1}{2}}}{\Delta x} - j^{n+\frac{1}{2}}_{y,j} \tag{25c}$$

at grid-point j, where the different field quantities are evaluated at the grid as shown in Fig. 6. The transverse fields are updated analogously.

The processes described above can be solved in a numerically stable way on a 1D grid [9, 10]. By adding and subtracting Maxwell's equations in Eq. (24) elementwise it is possible to obtain

$$(\partial_t - c\partial_x)(E_y - cB_z) = -j_y \tag{26a}$$
$$(\partial_t + c\partial_x)(E_y + cB_z) = -j_y \tag{26b}$$
$$(\partial_t - c\partial_x)(E_z + cB_y) = -j_z \tag{26c}$$
$$(\partial_t + c\partial_x)(E_z - cB_y) = -j_z \tag{26d}$$

that are combined together as

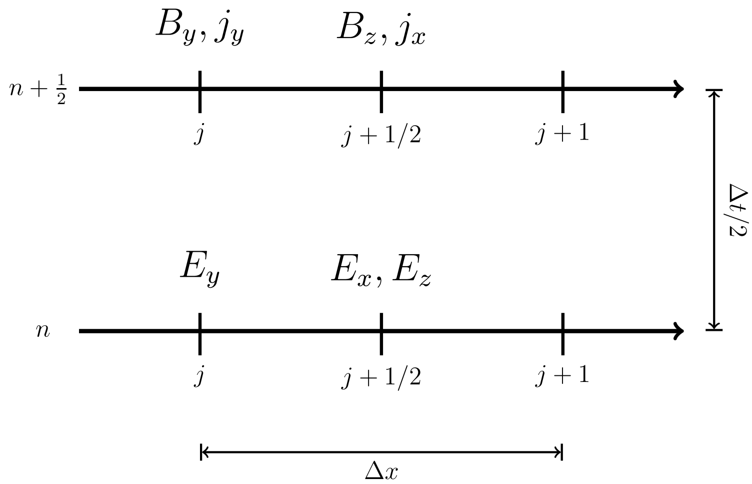

Figure 6: Field components on time and space grid in leap-frog scheme, where the electric field is computed on integer time steps and the magnetic field on half-integer time steps.

$$(\partial_t \pm c\partial_x)F^{\pm} = -\frac{1}{2}j_y \tag{27a}$$

$$(\partial_t \mp c\partial_x)G^{\pm} = -\frac{1}{2}j_z \tag{27b}$$

where F^+ and G^- are defined as *right-going* and F^- and G^+ as *left-going* field quantities and are given by

$$F^{\pm} = \frac{1}{2}(E_y \pm cB_z) \tag{28a}$$

$$G^{\pm} = \frac{1}{2}(E_z \pm cB_y) \tag{28b}$$

These can be computed separately, and to obtain the electromagnetic fields again

$$E_y = F^+ + F^-, cB_z = F^+ - F^- \tag{29a}$$

$$E_z = G^+ + G^-, cB_y = G^+ - G^- \tag{29b}$$

Eq. (24a) is discretized as

$$F^{\pm}(x \pm \Delta x, t + \Delta t) - F^{\pm}(x,t) = \frac{1}{2}j_y^{\pm}(x \pm \frac{\Delta x}{2}, t + \frac{\Delta t}{2}) \tag{30}$$

where $j_y^{\pm}$ is the averaged current that is space- and time centered. Eq. (29a) is discretized analogously. The grid spacing Δx is given by $\Delta x = c\Delta t$ which is a necessary condition due to vacuum dispersion according to [9, 10]. The other left- and right-going field quantities are discretized analogously. Updating the fields at grid point j from time step t_n to t_{n+1} is computationally carried out by

$$F_j^{\pm}(n+1) = F_{j\mp1}^{\pm}(n) - \frac{\Delta t}{4}(j_{y,j\mp1}^{-} + j_{y,j}^{+}) \tag{31a}$$

$$G_j^{\pm}(n+1) = G_{j\pm1}^{\pm}(n) - \frac{\Delta t}{4}(j_{z,j\pm1}^{-} + j_{z,j}^{+}) \tag{31b}$$

where $j_{y,j}^{-}$ is the current density in the y-direction at grid point j computed from the particle positions and velocities at time t_n and $t_{n+\frac{1}{2}}$ respectively. The current density $j_{y,j}^{+}$ is computed from the the particle positions after the particle push at time t_{n+1} and their respective velocities at time $t_{n+\frac{1}{2}}$.

2.3.5 Computation of the Lorentz Force

In electromagnetic cases the cross-term in the Lorentz force $\mathbf{F} = q\mathbf{E} + \frac{\mathbf{u}\times\mathbf{B}}{\gamma}$ (where $\mathbf{u} \equiv \gamma\mathbf{v}$) is not very straightforward to compute. Using finite differences turns the relativistic version of the Lorentz Force (Eq. (1)) into

$$\frac{\mathbf{u}^{n+\frac{1}{2}} - \mathbf{u}^{n+\frac{1}{2}}}{\Delta t} = \frac{q}{m}\left[\mathbf{E}^n + \frac{1}{c}\frac{\mathbf{u}^{n+\frac{1}{2}} + \mathbf{u}^{n+\frac{1}{2}}}{2\gamma^n} \times \mathbf{B}^n\right] \tag{32}$$

where $\mathbf{u}^{n+\frac{1}{2}}$ and γ^n are unknown. To compute this the *Boris method* is often used [9], which separates the electric and magnetic contributions to the force by defining

$$\mathbf{u}^{n-\frac{1}{2}} = \mathbf{u}^{-} - \frac{q\mathbf{E}^n\Delta t}{2m} \tag{33a}$$

$$\mathbf{u}^{n+\frac{1}{2}} = \mathbf{u}^{+} + \frac{q\mathbf{E}^n\Delta t}{2m} \tag{33b}$$

which is an advancement of the momentum $\frac{\Delta t}{2}$. Putting these expressions of $\mathbf{u}^{n-\frac{1}{2}}$ and $\mathbf{u}^{n+\frac{1}{2}}$ into Eq. (32) yields

$$\frac{\mathbf{u}^{+} - \mathbf{u}^{-}}{\Delta t} = \frac{q}{mc}\left[\frac{\mathbf{u}^{+} + \mathbf{u}^{-}}{2\gamma^n} \times \mathbf{B}^n\right] \tag{34}$$

which cancels out $\mathbf{E}$ and left is a rotation of $(\mathbf{u}^{-} + \mathbf{u}^{+})$. This rotation is computed in two steps as

$$\mathbf{u}' = \mathbf{u}^- + \mathbf{u}^- \times \mathbf{t} \tag{35a}$$
$$\mathbf{u}^+ = \mathbf{u}^- + \mathbf{u}' \times \mathbf{s} \tag{35b}$$

where

$$\mathbf{t} = \frac{q\mathbf{B}^n \Delta t}{2\gamma^n mc} \tag{36a}$$
$$\mathbf{s} = 2\frac{\mathbf{t}}{1+t^2} \tag{36b}$$

The Lorentz factor γ^n in the equations above is given by

$$\gamma^n = \sqrt{1 + (\frac{u^-}{c})^2} \tag{37}$$

Once $\mathbf{u}^+$ is computed Eq. (33b) is used to obtain $\mathbf{u}^{n+\frac{1}{2}}$. Note that Eq. (32) requires $\mathbf{B}^n$ at integer time steps rather than $\mathbf{B}^{n+\frac{1}{2}}$ obtained from the leapfrog scheme. Time averaging of the magnetic field is performed by

$$\mathbf{B}^n = \frac{\mathbf{B}^{n-\frac{1}{2}} + \mathbf{B}^{n+\frac{1}{2}}}{2} \tag{38}$$

which gives $\mathbf{B}^n$ at integer time steps.

3 Simulations

The experimental setup that was simulated in this project is illustrated in Fig. 1: a short high-intensity laser pulse of of a few wavelengths was irradiated onto a slab of plasma with an incidence angle θ to the normal of the plasma boundary. The incident wave interacted with the plasma particles and in the process they emitted radiation of a certain characteristic.

The dynamics of the plasma particles depend mainly on the incidence angle θ, the phase-shift Ψ and three ratios. One is the ratio between the plasma frequency ω_p and the laser frequency ω_L. The second is between the amplitude of the incident electric field a_0 and the laser frequency ω_L, and the third is the ratio between the amplitudes of the electromagnetic field components. The following parameters are sufficient in determining the three ratios described above:

- $S = \frac{n_0}{n_c a_0}$, known as the relativistic similarity parameter. The field amplitude in relativistic, dimensionless units is defined as $a_0 = a_0(a_{y,0}, a_{z,0}, \Psi) = \max\left(\sqrt{a_{y,L}^2(x,t) + a_{z,L}^2(x,t)}\right)$.
- $I\lambda^2 = a_0^2 \cdot 1.37 \cdot 10^{18} \mu\text{m}^2/\text{cm}^2$, which decides the intensity of a p-polarized pulse. Setting $a_0 = 85$ yields a laser intensity of $\sim 10^{22}$ W/cm^2 for for a p-polarized laser with a wavelength of $\lambda = 1\mu$m [10]. The intensity is doubled for a circularly polarized wave since the pulse amplitude does not oscillate in time [5].
- $a_{y_0}/a_{z,0}$ determines the polarization of the wave together with Ψ. For $\Psi = \pi/2$, $a_{y,0}/a_{z,0} = 1$ corresponds to circular polarization, $a_{y,0}/a_{z,0} \neq 1$ to elliptical polarization and $a_{z,0} = 0$ to p-polarization.

A few different experimental setups was simulated throughout this project. The general simulation was of the laser-plasma interaction of a short laser pulse with intensity I, angular frequency ω_L with an incidence angle θ to the normal of the plasma boundary (see Fig. 1). The amplification $a'_{i,g}/a'_0$ (for $i = \{y,z\}$) of the emitted pulse was computed as a function of incident angle θ and the similarity parameter S. This was done for an incident pulse of linear as well as circular polarization. Simulations were run for arbitrary polarization as well but with a fixed S and θ with the aim to study the agreement with the RES-AP model.

3.1 Particle-in-cell simulations

All PIC simulations were carried out with a code written in Fortran 90 in this project. It is a 1D PIC code that can be used to simulate high-intensity laser-plasma interactions at oblique incidence and arbitrary pulse polarization. The particles were initially distributed uniformly in the plasma domain with assigned particle velocity-components from a relativistic Maxwellian distribution which were Lorentz transformed into the moving frame as in Sec. 2.2.1.

Simulations scanning the parameter space spanned by $S \in [0.1,4]$ and $\theta \in [0°,80°]$ were performed for a pulse of p-polarization as well as left- and right-going circular polarization. The incident pulse had a length of $2\lambda'_L$ ($3\lambda'_L$) and the simulations were run for 2.5 (4.5) wave periods for a p-polarized wave (circularly polarized wave). The length of the plasma L at $t = 0$ was initiated to $L = 2\lambda'_L$ ($L = 4\lambda'_L$). These parameter values were chosen so that the plasma density close to the non-active boundary was remained unperturbed for each choice of S, θ and that at least two uniform wavelengths of the laser had interacted with the plasma.

In this project only two values of the laser intensity was used in the PIC simulations: $a_0 = 85$ ($a_0 = 42.5$ for circular polarization) and $a_0 = 191.1$ corresponding to intensities of 10^{22} W/cm^2 and $5 \cdot 10^{22}$ W/cm^2 respectively, which are the intensities state-of-the-art facilities are able to produce today.

3.2 Simulations of the RES-AP model

The differential equations in the derived physical model RES-AP were simulated using MATLAB. The Euler method was used to update the position of the particle in the boundary layer from Eq. (16). The velocities were obtained by minimizing Eqs. (13) on a grid using the relation given in Eq. (17). The relativistic factor parameter γ_p was set to $\gamma_p = 5$.

4 Results

The results from the numerical simulations are presented next to those expected from the Relativistic Electron Spring model described in Sec. 2.2.2. Results from simulations is also presented with the aim to justify the assumptions made when deriving the RES-AP model.

4.1 Linear polarization

Snapshots of the electric field $a'_{y,g}/a'_0$ for a p-polarized wave at three different stages are shown in Fig. 7; one at $t' = 0$, one at the maximum displacement of the plasma boundary $t' = 1.44T'_L$ (T'_L is the period time of the incident wave in the moving frame) and one at the last time step of the simulation at $t' = 2.5T'_L$. The incidence angle and similarity parameter used for Fig. 7 were also the parameters generating the maximum field amplification ($\theta = 62°$ and $S = 0.375$). The plasma density at the same time steps are shown in Fig. 8.

Depending on the values of $\{S,\theta\}$ the shape of the back-radiated pulse varied. Three different types of pulse shapes were observed and examples from the PIC simulations are shown in Fig. 9.

The maximum amplification of the re-emitted pulse for two different intensities $I = 10^{22}$ W/cm^2 and $I = 5 \cdot 10^{22}$ W/cm^2 are shown in Fig. 10, where both intensities yields similar results in the $\{S,\theta\}$ plane with maximum amplification obtained at $\theta = 62°$ and $S = 0.35$.

As illustrated in Fig. 7 and 9 the duration of the backscattered pulse is considerably shorter than that of the incident wave.

4.2 Circular polarization

Simulations were performed for incidents waves of both left- and right-going circular polarization. They yielded very similar results why only results from the right-going case are presented.

A corresponding figure for right-going circular polarization as in Fig. 7 illustrating the time evolution of the simulation is shown in Fig. 11.

The maximum amplification of the y- and z-components of the electric field as a function of θ and S are shown in Fig. 12.

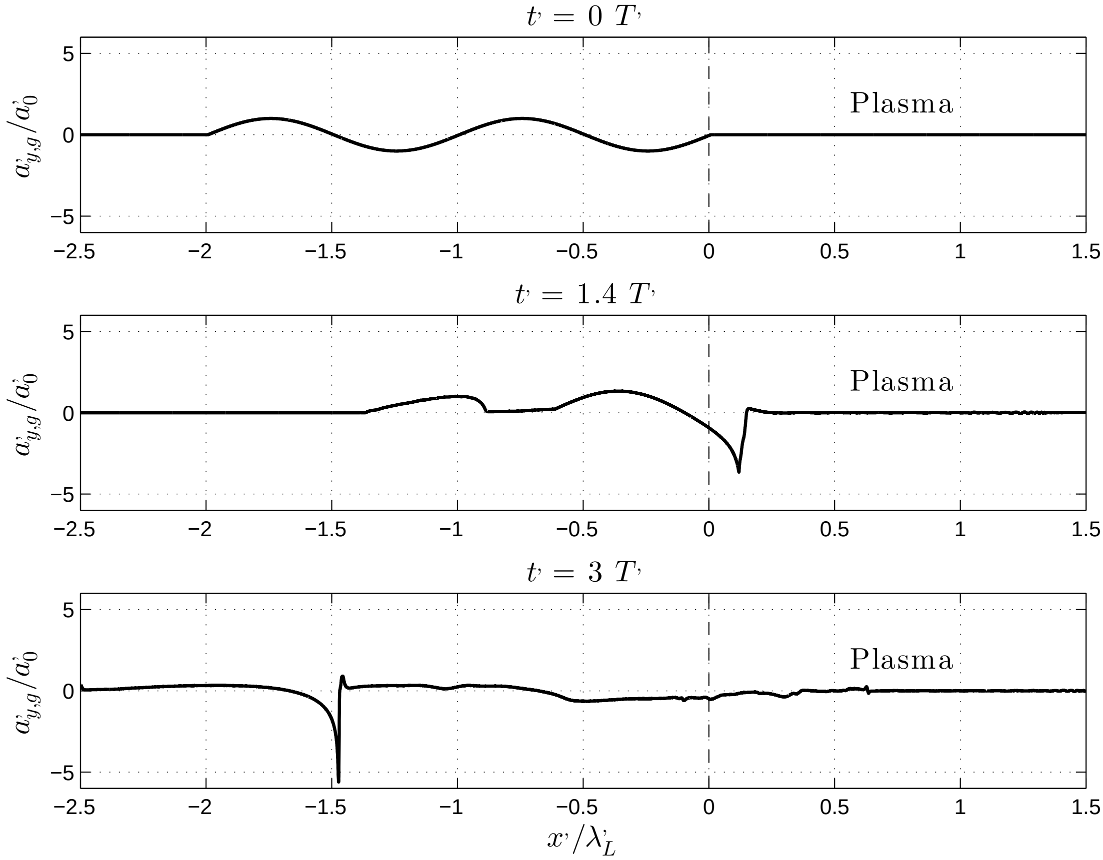

Figure 7: Shows the state of the normalized y-component of the electric field at three different stages in the moving frame. The first plot is at $t = 0$ at the start of the interaction, the second is at the maximum displacement of the boundary layer, and the third is after 2.5 wave periods of the incident pulse have passed. The results are obtained from a PIC simulation with $a_{y,0} = 85$ (corresponding to $I = 10^{22}$ W/cm^2 for $\lambda = 1\mu$m), plasma thickness $L = 2\lambda'$, $\Delta t = \Delta x = 0.05\omega_p$, similarity parameter $S = 0.375$, incident angle $62°$ and 50 particles per cell.

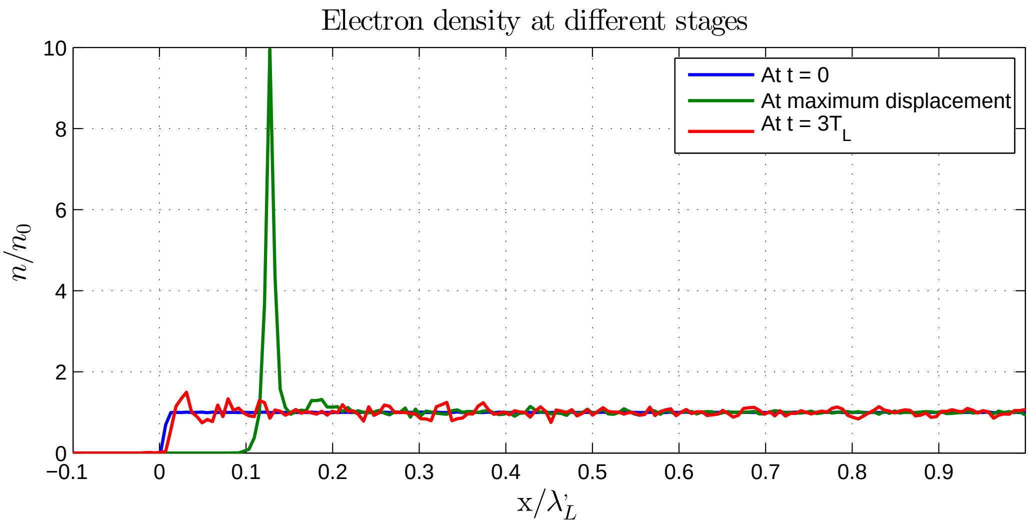

Figure 8: Plasma density for the same three time steps as in Fig. 7. Note the boundary layer present at the maximum displacement (green). The results are obtained from a PIC simulation with $a_{y,0} = 85$ (corresponding to $I = 10^{22}$ W/cm^2 for $\lambda = 1\mu$m), plasma thickness $L = 2\lambda'$, $\Delta t = \Delta x = 0.05\omega_p$, similarity parameter $S = 0.375$, incident angle 62° and 60 particles per cell.

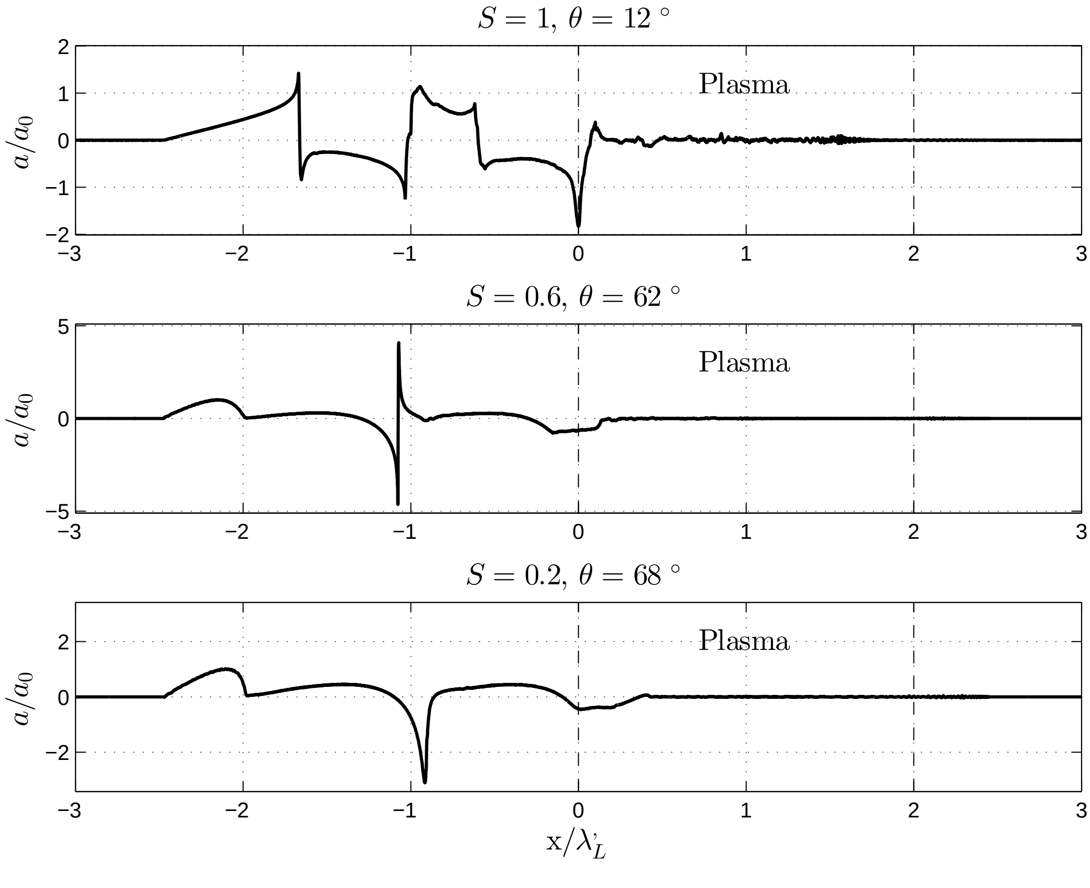

Figure 9: Pulse shapes of back-radiated pulses at $T = 2.5T$ obtained from PIC simulations for different combinations of incident angle θ and similarity parameter S. The simulation parameters used were $a_{y,0} = 85$ (corresponding to $I = \cdot 10^{25}$ W/cm^2 for $\lambda = 1\mu$m), plasma thickness $L = 2\lambda'_L$, $\Delta t = \Delta x = 0.1\omega_p$ for 30 macroparticles per cell.

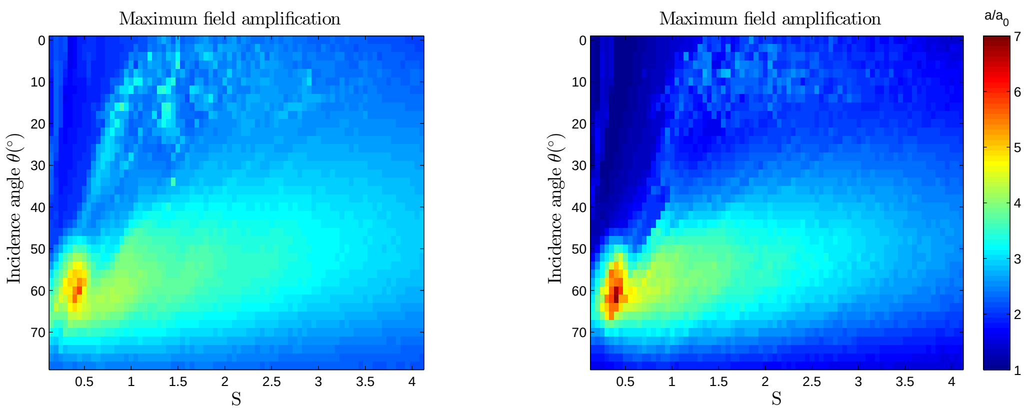

Figure 10: Electric field amplification obtained for $a_{y,0} = 85.0$ (left) and $a_{y,0} = 191.1$ (right) corresponding to $I = 10^{22}$ and $I = 5 \cdot 10^{22}$ W/cm^2 respectively for $\lambda = 1\mu$m. Results obtained from PIC simulations with varying incident angle θ and similarity parameter S. The simulation parameters used were plasma thickness $L = 2\lambda_L'$, $\Delta t = \Delta x = 0.1\omega_p$ for 30 macroparticles per cell.

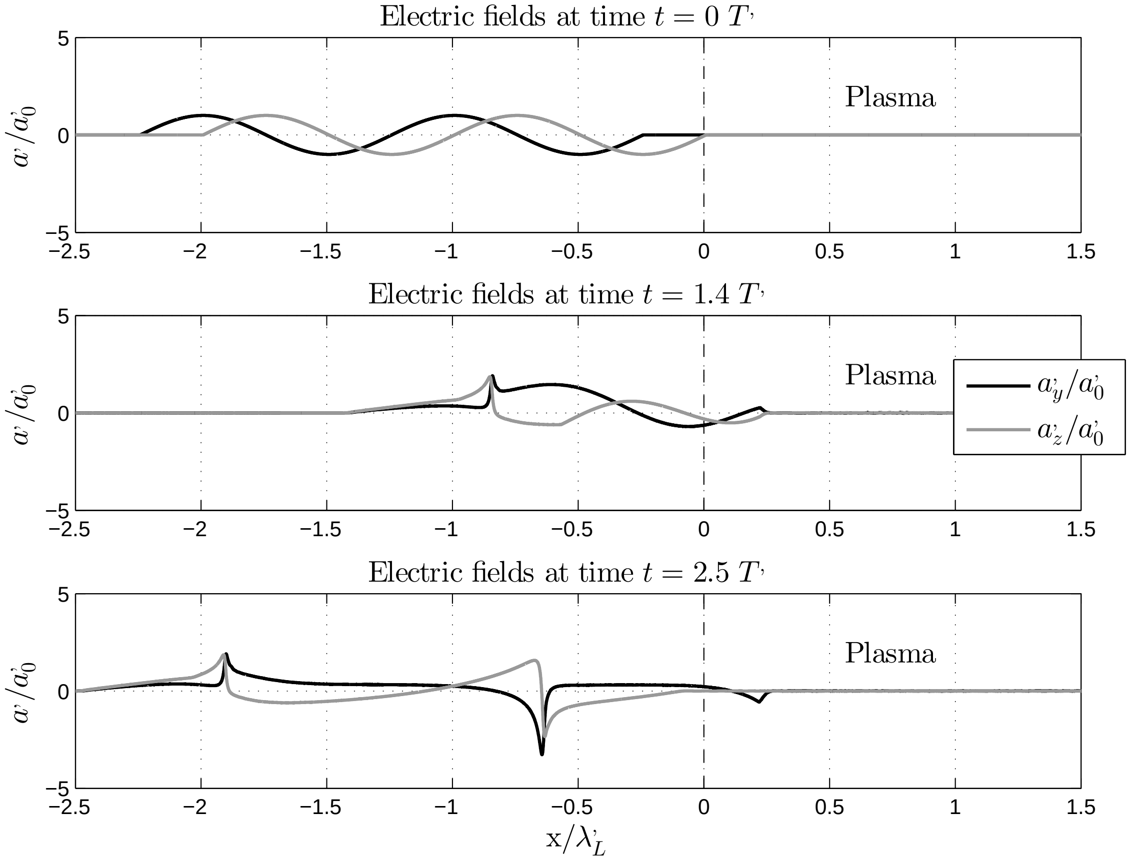

Figure 11: Shows the state of the normalized y- (black) and z-component (gray) of the electric field at three different stages in the moving frame. The first plot is at $t = 0$ at the start of the interaction, the second is at the maximum displacement of the boundary layer, and the third is after 2.5 wave periods of the incident pulse have passed. The results are obtained from a PIC simulation with $a_{y,0} = 85$ (corresponding to $I = \cdot 10^{22}$ W/cm^2 for $\lambda = 1\mu$m), plasma thickness $L = 2\lambda'$, $\Delta t = \Delta x = 0.05\omega_p$, similarity parameter $S = 0.375$, incident angle 62° and 60 particles per cell.

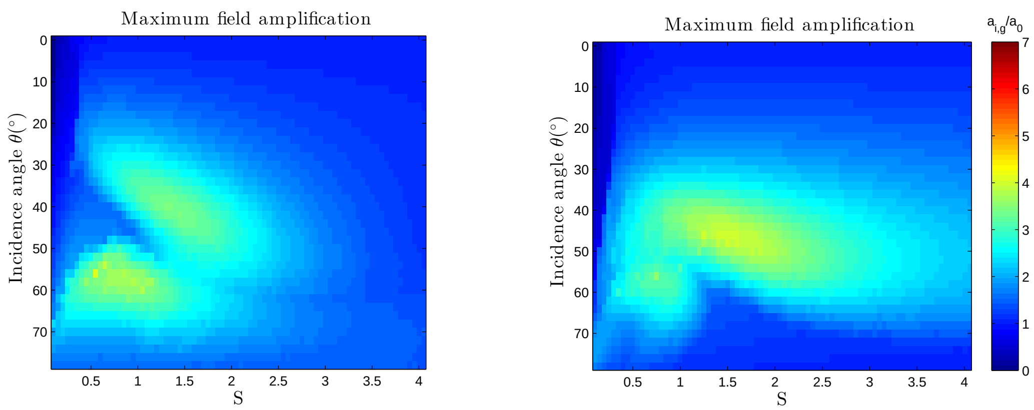

Figure 12: Maximum amplification of y- (left) and z-component (right) of electric field obtained from PIC simulations with varying incident angle θ and similarity parameter S for a right-going circular polarized laser. The simulation parameters used were $a_{y,0} = a_{z,0} = 42.5$ (corresponding to $I = \cdot 10^{22}$ W/cm^2 for $\lambda = 1\mu$m), plasma thickness $L = 4\lambda'$, $\Delta t = \Delta x = 0.1\omega_p$ for 40 macroparticles per cell.

4.3 Comparison of PIC simulations and theoretical model

Simulations of the dynamics of the RES-AP model were performed and compared to the results obtained from the PIC simulations. In Fig. 13 and 14 the reemitted pulses are shown from a p- and a circularly polarized wave respectively, and the maximum amplification as a function of S and θ obtained from the RES-AP model is presented in Fig. 15 and Fig. 16

The dynamics of the boundary layer obtained from the RES-AP model is plotted together with the plasma density from the PIC simulations in Fig. 17 and 18.

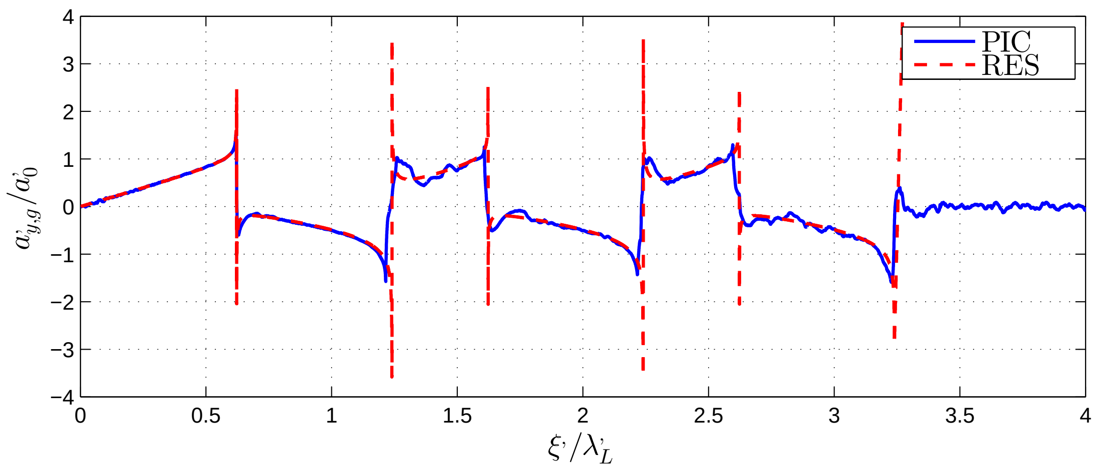

Figure 13: The y-component of electric field obtained from PIC simulations (solid) and the RES-AP model (dashed) for a p-polarized laser. The simulation parameters used were $\theta = 12°$, $S = 2$, $a_{y,0} = 85.0$ (corresponding to $I = 10^{22}$ W/cm^2 for $\lambda = 1\mu$m), plasma thickness $L = 2\lambda'$, $\Delta t = \Delta x = 0.05\omega_p$ for 50 macroparticles per cell. For the RES-AP simulation $\gamma_p = 5$ was used.

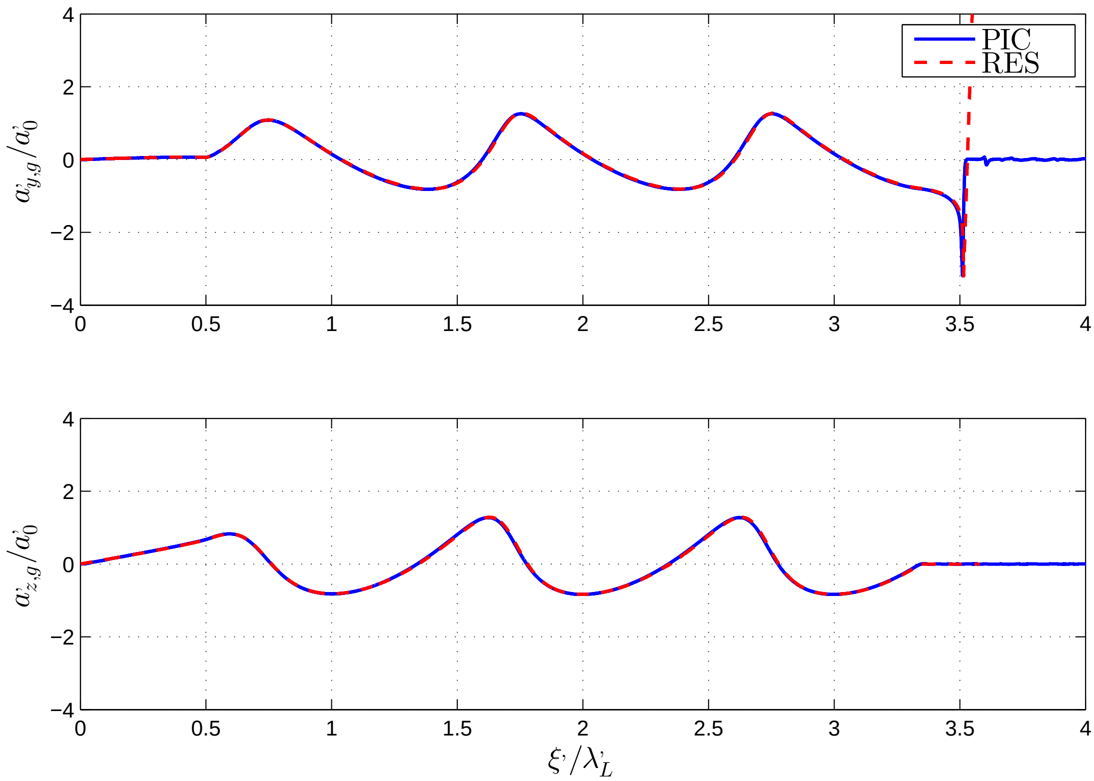

Figure 14: The y- (top) and z-component (bottom) of the electric field obtained from PIC simulations (solid) and the RES-AP model (dashed) for a right-going circularly polarized laser. The simulation parameters used were $\theta = 12°$, $S = 2$, $a_{y,0} = 85.0$ (corresponding to $I = 2 \cdot 10^{22}$ W/cm^2 for $\lambda = 1\mu$m), plasma thickness $L = 2\lambda'$, $\Delta t = \Delta x = 0.05\omega_p$ for 50 macroparticles per cell. For the RES-AP simulations $\gamma_p = 5$ was used.

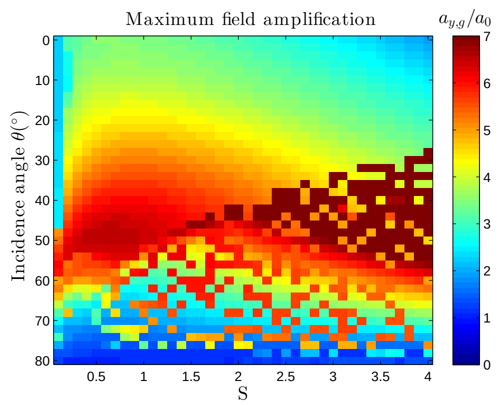

Figure 15: Maximum amplification of the y-component of the electric field obtained from the RES-AP model with varying incident angle θ and similarity parameter S for a p-polarized wave. The relativistic gamma parameter was set to $\gamma_p = 5$.

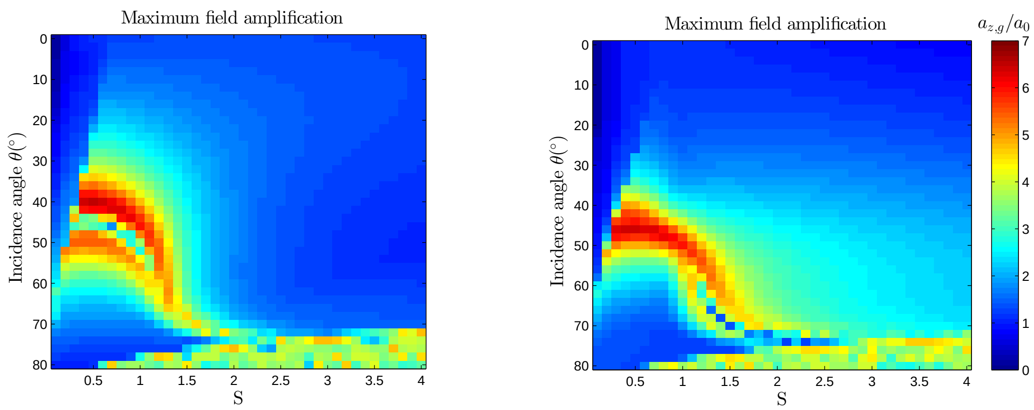

Figure 16: Maximum amplification of the y- (left) and z-component (right) of electric field obtained from the RES-AP model with varying incident angle θ and similarity parameter S for a right-going circular polarized laser. The relativistic gamma parameter was set to $\gamma_p = 5$.

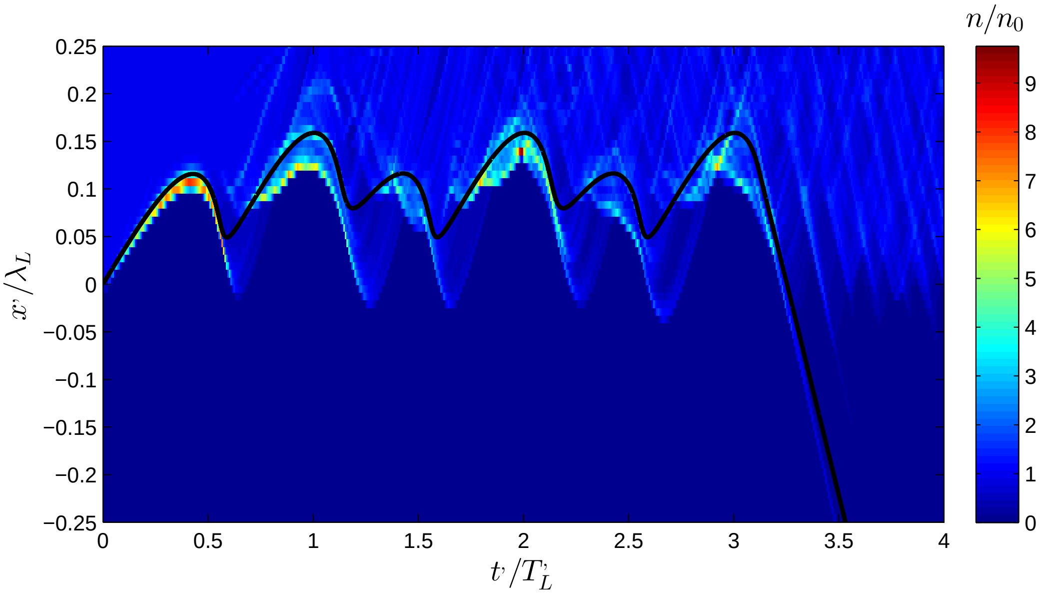

Figure 17: The time evolution of the plasma density obtained from PIC simulations compared with the dynamics of the boundary layer obtained from the RES-AP model (black line) for an incident wave of p-polarization. The PIC simulation parameters used were $\theta = 12°$, $S = 2$, $a_{y,0} = 85.0$ (corresponding to $I = 10^{22}$ W/cm^2 for $\lambda = 1\mu$m), plasma thickness $L = 2\lambda'$, $\Delta t = \Delta x = 0.02\omega_p$ for 100 macroparticles per cell. For the RES-AP simulations $\gamma_p = 5$ was used.

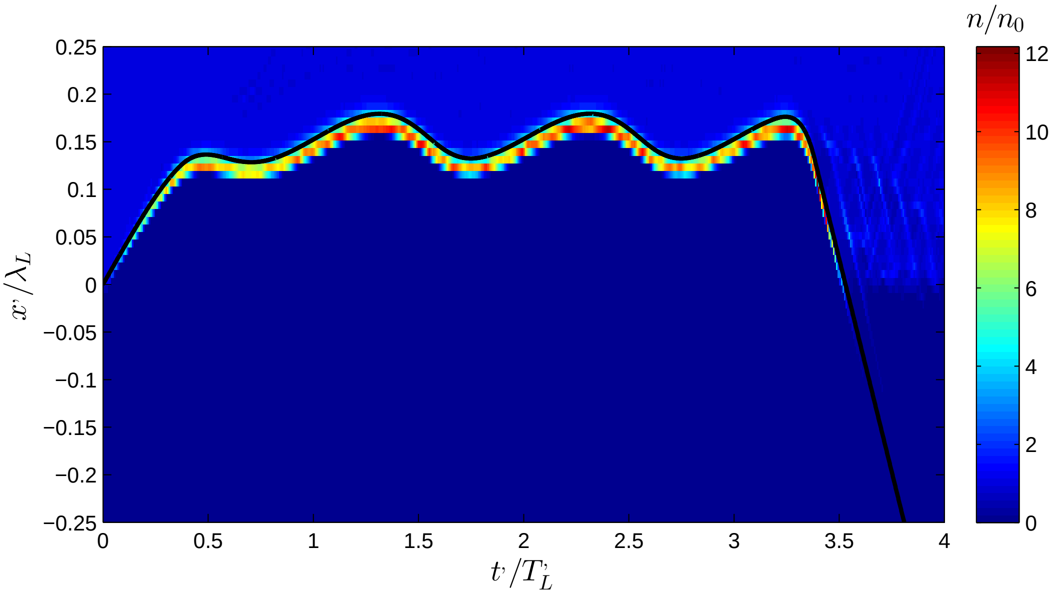

Figure 18: The time evolution of the plasma density obtained from PIC simulations compared with the dynamics of the boundary layer obtained from the RES-AP model (black line) for an incident wave of right-going circular polarization. The PIC simulation parameters used were $\theta = 12°$, $S = 2$, $a_{y,0} = a_{z,0} = 85.0$ (corresponding to $I = 2 \cdot 10^{22}$ W/cm^2 for $\lambda = 1\mu$m), plasma thickness $L = 2\lambda'$, $\Delta t = \Delta x = 0.02\omega_p$ for 100 macroparticles per cell. For the RES-AP simulation $\gamma_p = 5$ was used.

For lower plasma densities (corresponding to lower values of $\sim S < 0.5$) it was observed that the plasma boundary could be pushed back further and further in each wave cycle but that the boundary layer splits up in the process. For these parameter values the results from the RES-AP model did not always correspond very well with the PIC simulations. These two phenomenas are illustrated in Fig. 19 and Fig. 20.

The effect of the choice of the relativistic factor γ_p in the RES-AP simulations is illustrated in Fig. 21. A sufficiently large γ_p yielded a good curve fit but also increased the maximum amplification in the asymptotic regions.

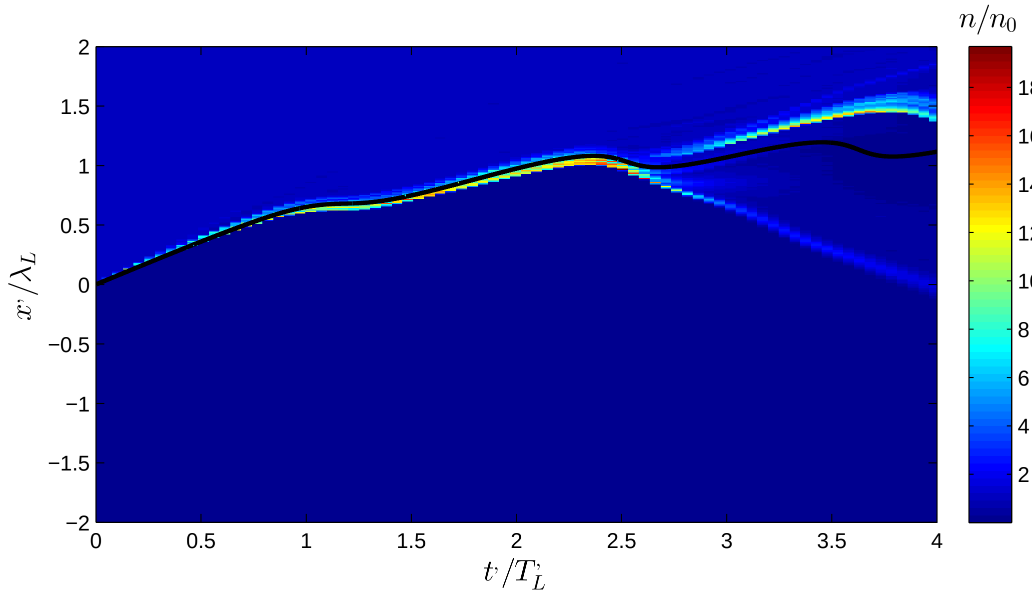

Figure 19: The time evolution of the plasma density obtained from PIC simulations compared with the dynamics of the boundary layer obtained from the RES-AP model (black line) for an incident wave of right-going circular polarization. The PIC simulation parameters used were $\theta = 12°$, $S = 0.2$, $a_{y,0} = a_{z,0} = 85.0$ (corresponding to $I = 2 \cdot 10^{22}$ W/cm^2 for $\lambda = 1\mu$m), plasma thickness $L = 4\lambda'$, $\Delta t = \Delta x = 0.02\omega_p$ for 100 macroparticles per cell. For the RES-AP simulation $\gamma_p = 5$ was used.

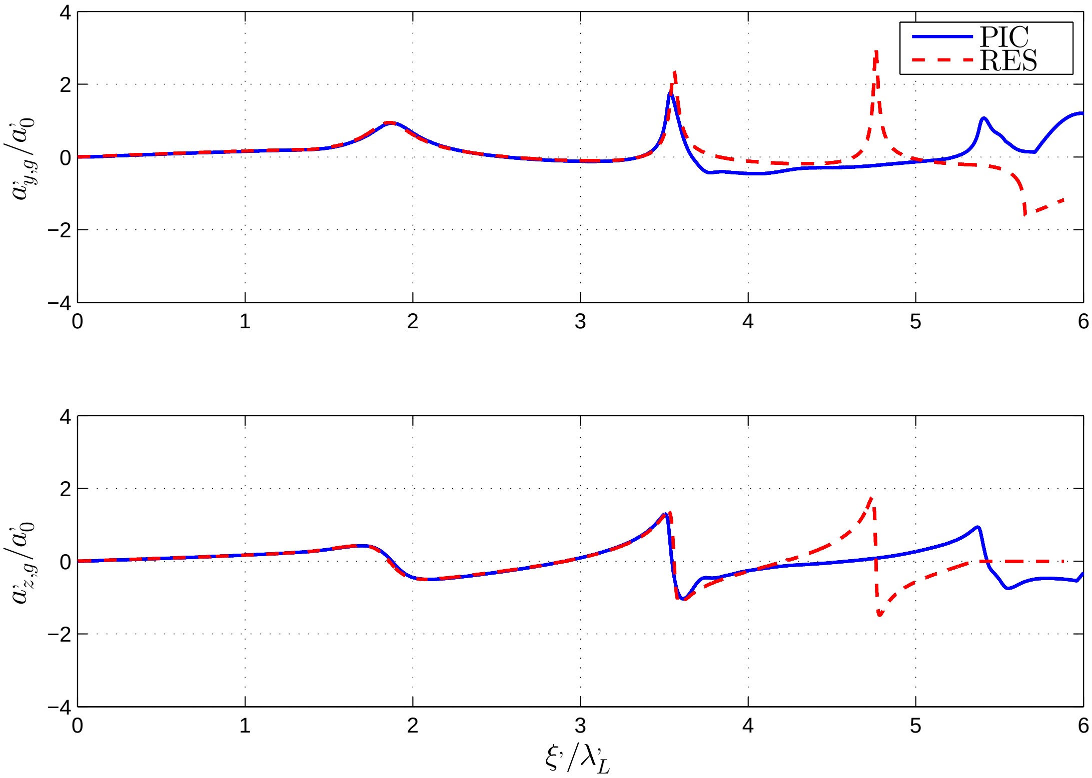

Figure 20: The y- (top) and z-component (bottom) of the electric field obtained from PIC simulations (solid) and the RES-AP model (dashed) for a right-going circularly polarized laser. The simulation parameters used were $\theta = 30°$, $S = 0.2$, $a_{y,0} = a_{z,0} = 85.0$ (corresponding to $I = 2 \cdot 10^{22}$ W/cm^2 for $\lambda = 1\mu$m), plasma thickness $L = 4\lambda'$, $\Delta t = \Delta x = 0.1\omega_p$ for 50 macroparticles per cell. For the RES-AP simulation $\gamma_p = 5$ was used.

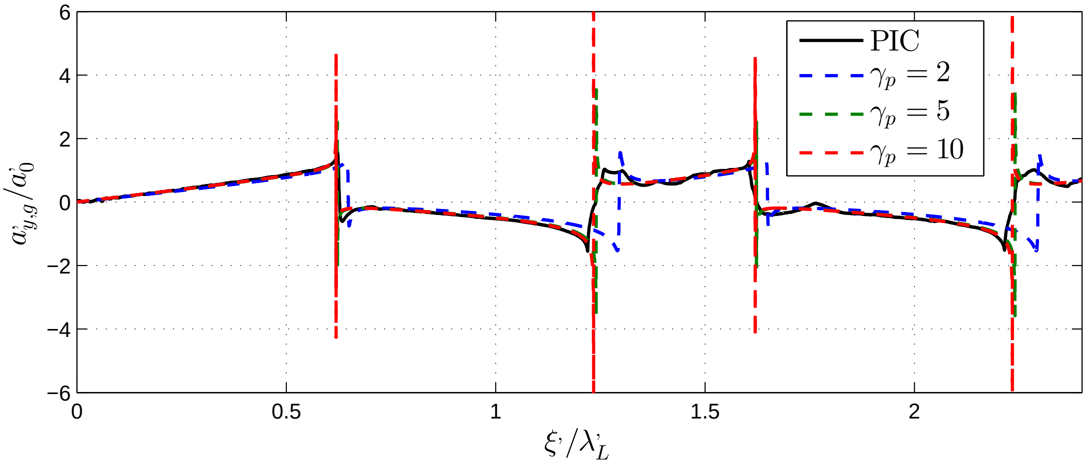

Figure 21: The y-component of the electric field obtained from PIC simulations (solid, black) for a p-polarized incident laser and the RES-AP model (dashed) for different values of γ_p. The parameters used in the PIC simulations were $\theta = 12°$, $S = 0.2$, $a_{y,0} = 85.0$ (corresponding to $I = 10^{22}$ W/cm^2 for $\lambda = 1\mu$m), plasma thickness $L = 5\lambda'$, $\Delta t = \Delta x = 0.05\omega_p$ for 50 macroparticles per cell.

5 Discussion

The results from the Particle-in-cell simulations were in general in good agreement with the theoretical model and are discussed further in Sec. 5.1 and Sec. 5.2. The possible ways to improve the accuracy of the simulations are covered in Sec. 5.3 and future simulations are suggested in Sec. 5.5

5.1 PIC simulations

Irradiating the plasma boundary with p-polarized laser generated a greater maximum amplification of the incident wave than circularly polarized (CP) laser did. This can be explained intuitively by that polarization the incident sinusoidal $a'_{y,L}$ and $a'_{z,L}$ fields are shifted with $\Psi = \pi/2$ in respect to each other, which means that $a'_{z,L}|_{a'_{y,L}=a'_0} = 0$ and $a'_{z,L}|_{a'_{y,L}=0} = a'_0$. When $a'_{y,L}(t,x_b) \to 0$ at the plasma boundary is when $\beta_x \to -1$ for the p-polarized wave. However, in the case of a CP wave $|\beta_z|$ is forced $\to 1$ as $\beta_y \to 0$ which interferes with $\beta_x \to -1$ since $|\mathbf{v}| < c$. The asymptotic shape of the re-emitted pulse that is obtained from a p-polarized wave and gives rise to the greatest amplifications in the $\{S,\theta\}$ plane is not as prominent in the CP case.

For a circularly polarized wave the plasma electrons are pushed tightly together throughout almost the entire time of interaction. The last $\lambda'/4$ of the pulse when $a'_{z,L} = 0$ is when the velocity of the electrons are free to approach $\beta_x \to -1$ and possibly generate a short, greatly amplified pulse. An example of this is seen in Fig. 14 and 18 at $t' \approx 3T'$. When either $a'_{y,L}$ or $a'_{z,L} \neq 0$ at the plasma boundary the energy from the incident circularly polarized wave is transferred to the plasma particles without the possibility to release the energy until the last $\lambda'/4$ of the pulse remains and $a'_{z,L} = 0$. For lower values of S (and hence a lower plasma density) the incident wave can in fact push back the boundary further and further in every cycle of the wave and thus accumulate even more energy in the plasma. This phenomena is discussed further in Sec. 5.5

5.2 Comparison with the theoretical model

The general impression was that the RES-AP model was in good agreement with the Particle-in-cell simulations performed, especially when it came to describing the characteristics of the emitted radiation (Fig. 13 and 14). Both the y- and z-components of the radiation pattern looked very similar to the ones obtained from the PIC simulations. It had limitations however in predicting the maximum amplitude from the radiation bursts. For many choices of (θ, S) the bursts showed asymptotic behavior, and the amplitude of those were highly dependent on the choice of Lorentz factor γ_p. The value of γ_p should ideally be a function of S, θ and

a_0, since all of these parameters affect the energy transferred to a plasma particle and by that the velocity of the particles. Increasing a_0 for instance corresponds to a greater intensity of the incident wave which results in velocities even closer to c which means that γ increases as a_0 increases. In Fig. 10 it can be seen that $a_0 = 191.1$ gives a greater maximum amplification than $a_0 = 85$ which is connected to the increase in relativist effects the greater particle velocities give rise to. In the RES-AP model this is explained by that Eq. (18) becomes singular as $\beta_x \to -1$ and the greater γ_p is the closer β_x can get to -1. The difficulties in assigning γ_p which affected the particle dynamics at the singularity point $\beta_x \to -1$ (see Fig. 21) made it problematic to construct corresponding plots to Fig. 10 and 12 for the RES-AP model.

It should be noted that the dynamics of the boundary layer is not affected by the value of γ_p, given that it is sufficiently large. The effect of γ_p is seen clearly in Fig. 21, where $\gamma_p = 2$ gives radiation peaks that doesn't correspond to those obtained from the PIC simulations. This means that the movement of the plasma boundary is incorrect, and can be explained by the fact that $\gamma_p = 2$ gives a maximum electron speed of $|\beta|_{\max} = \sqrt{3/4} \approx 0.866$ which heavily affects the dynamics. For $\gamma_p = 5$ and $\gamma_p = 10$ the layer dynamics are very similar to the PIC results since the radiation peaks occurs at the same positions. This is due to that $\gamma_p = 5$ and $\gamma_p = 10$ corresponds to maximum particle velocities of $|\beta|_{\max} \approx 0.980$ and $|\beta|_{\max} \approx 0.995$ respectively and the most prominent difference between the radiation patterns are the maximum values of the radiation pattens in the singular points. By looking at Eq. (13) and Eq. (18) it is easy to explain this behavior. For Eq. (13) describing the boundary dynamics the factor $\frac{1}{1-\beta_x}$ is present and how close $\beta_x \to -1$ does not affect this factor very much as long as β_x gets sufficiently close to -1. The value of the factor $\frac{1}{1+\beta_x}$ on Eq. (18) depends heavily on how close β_x gets to -1, which explains the vast difference in amplitude in the singular points.

The system of equations in the RES-AP model (13) assumes that all the electrons in the boundary layer move collectively when emitting the radiation and that it completely compensates for the incident radiation. In Fig. 17 and 18 it is seen in the density plots that there has formed a single boundary layer in the CP case that is not as distinct in the p-polarized case. One of the main assumptions in RES-AP model is that all electrons left of a moving boundary point is pushed together to form a single boundary layer and move collectively. That behavior is clearly seen in the circularly polarized case and is why the re-emitted radiation in Fig. 14 is much smoother and coherent than for the p-polarized wave in Fig. 13. The maximum field amplification obtained from the PIC simulations (Fig. 10 and 12) and the RES-AP model (Fig. 15 and 16) showed a better agreement for the CP wave than for the p-polarized wave, and the poor agreement is a consequence of the too generous assumptions in the RES model discussed above.

5.3 Comments about the Particle-in-cell simulations

In this project a few approximations were made due to numerical reasons. The ions were assumed stationary because of the difference in mass by a factor $\sim Z \cdot 10^3$ which would slow down the acceleration of the ions greatly. Hence it should not have affected the overall radiation characteristics (pulse shapes, boundary dynamics, etc.) but it is possible that the ions small movements could have a small effect on the electron velocity when approaching $\beta_x \to -1$ and could therefor alter the maximum field amplification slightly. For these short pulses the ions would not have the time to move a noticeable distance compared to the electrons, which could be shown numerically. However, for longer laser pulses of several wavelengths the ions would be able to shift their positions during the interaction. This would mean that the ions would oscillate at a frequency different to the one of the electrons, which could give rise to interesting phenomenons.

The particles were initially uniformly distributed in the plasma domain, which meant that the incident laser interacted with a sharp plasma boundary which is not very realistic. However, combining the results with the ones obtained from the RES-AP simulation - as well the arguments made when deriving the model - it should be clear that the high-intensity bursts of radiation comes from the relativistic motion of the particles and are not caused by the sharp plasma boundary.

The incident laser pulse were constructed by sinusoidal waves of one single frequency and the length of a few wave periods (see Fig. 3). A realistic laser pulse would not be 2λ long and completely sinusoidal. It would be longer and the shape of the pulse would not be step functions (as the dashed lines in Fig. 3) but have a rise time and a fall time. It was observed in the simulations that in the p-polarized case it did not matter how many λ:s the incident pulse consisted of in regards of giant pulse generation: the emitted radiation pattern was periodic. For the circular polarized case the plasma interaction of the last $\lambda/4$ of the pulse (where $E_z(x_b) = 0$) was often the event that emitted radiation of greatest intensity (as in Fig. 14). This behavior might hence not occur when a more realistic laser pulse collides with the plasma. Because of that the maximum amplification in Fig. 12 was not extracted from the radiation generated in the interaction with last $\lambda/4$ of the pulse.

5.4 Comparison with previous results

The results from the PIC simulations for the p-polarized laser pulse correspond very well with previous results [3]. The maximum amplification boost takes place at an incidence angle $\theta = 62°$ and similarity parameter $S = 0.375$ for a laser intensity of $5 \cdot 10^{22}$ W/cm^2 just as in [3]. These parameters gave a pulse amplification of $a_{y,g}/a_0 \approx 6.5$ and shortened the duration of the pulse by a factor $\sim 10^{-1}$ resulting in a radiation boost of $I_g/I_0 \sim 10^3$.

The Particle-in-cell code used in this project was developed independently of the one used in [5] where for instance a different numerical method was used for the field integration scheme. The fact that the results obtained in both research projects where so similar gives credibility to the results.

5.5 Future work

The generation of the high-intensity bursts of radiation has been showed through simulations in [3] and in this project, and it would be very interesting to see experimental results of the project. The experimental setup that has been simulated in the project with ideal laser pulses and uniform plasmas would differ in reality. More simulations should be made prior to performing this experimentally using more realistic pulse shapes and plasmas.

In this project only linear and circular polarization was simulated, but it is possible that an even greater field amplification can be achieved by another choice of polarization. The simulations would be time consuming, but the RES-AP model can be used to find areas in the (S,θ, $a_{y,0}/a_{z,0}$, Ψ)-space where the re-emitted pulses have asymptotic shapes. These areas would be the most likely to generate shortened, amplified pulses.

The RES-AP model proposed is still not perfect even tough it described the layer dynamics very well for most $\{S, \theta\}$. The main assumption that all electrons located $\in (0,x_s)$ forms a boundary layer and moves collectively gives a fairly good approximation but it is seen in for instance Fig. 17 that the electrons tends to split up into several layers. Incorporating this into the model would improve the results and give a better estimation of the layer dynamics as well as the emitted radiation. An analytic expression for the relativistic factor parameter γ_p as a function of S, a_0 and θ would probably make for a better prediction of the maximum field amplification.

In Sec. 5.3 it is discussed the effect of the the last $\lambda/4$ of the pulse, and how most of the energy accumulated in the plasma is released when interacting with this last part of the pulse. This opens up the concept of using two pulses to irradiate the plasma. The first pulse would be of circular polarization with the purpose to push the plasma boundary further and further back in each wave cycle and thus transfer more and more energy to the plasma. A second, linearly polarized wave would act as a "trigger" and make the plasma quickly release all its potential energy. Studying this numerically would require investigating the effects of additional parameters such as time gap between the two pulses and the ratio between the wavelengths of the two lasers. Together with the parameters S, θ

and a_0 it means that it would require very time consuming computations. To be able to carry out this study a parallelized PIC code would be necessary to run the simulations on a computing cluster.

6 Conclusion

In this project a Particle-in-cell code was developed to simulate laser-plasma interactions of laser intensities between $10^{21} - 10^{24}$ W/cm^2. Simulations with varying incident angle θ, similarity parameter S, incident field amplitude $\mathbf{a}_0$ were performed with incident lasers of p- as well as circular polarization. Linear polarization of the incident wave yielded a greater amplification of the re-emitted pulse than circular polarization. The greatest amplification was obtained at an incident angle $\theta = 62°$ and similarity parameter $S = 0.375$ which agrees with previous studies [3]. The results seems very promising as a route towards pulse intensities of 10^{25} W/cm^2 and the possibility to probe nonlinear effects in vacuum.

A theoretical framework describing the dynamics of these interactions was also developed by extendeding the Relativistic Electronic Spring model to apply to incident waves of arbitrary polarization. The theoretical model was in good agreement with the PIC simulations performed for linear and circular polarization.

The project verified previous simulations and the RES model derived in [5] by being able to reproduce the results. Future work would include extending the RES-AP model further, by for instance a better approximation of the γ_p parameter and by not limiting the electrons to move collectively in a single boundary layer in the model since PIC simulations showed that the boundary layer often split up.

References

[1] V. Yanovsky, V. Chvykov, G. Kalinchenko, P. Rousseau, T. Planchon, T. Matsuoka, A. Maksimchuk, J. Nees, G. Cheriaux, G. Mourou, K. Krushelnick, Ultra-high intensity- 300-tw laser at 0.1 hz repetition rate, Opt. Express 16 (3) (2008) 2109–2114.

[2] D. K. Cheng, et al., Fundamentals of engineering electromagnetics, Addison-Wesley Reading, MA, 1993.

[3] A. A. Gonoskov, A. V. Korzhimanov, A. V. Kim, M. Marklund, A. M. Sergeev, Ultrarelativistic nanoplasmonics as a route towards extreme-intensity attosecond pulses, Phys. Rev. E 84 (2011) 046403.
URL `http://link.aps.org/doi/10.1103/PhysRevE.84.046403`

[4] A. Bourdier, Oblique incidence of a strong electromagnetic wave on a cold inhomogeneous electron plasma. relativistic effects, Physics of Fluids (1958-1988) 26 (7) (1983) 1804–1807.
URL `http://scitation.aip.org/content/aip/journal/pof1/26/7/10.1063/1.864355`

[5] A. Gonoskov, Ultra-intense laser-plasma interaction for applied and fundamental physics, Ph.D. thesis, Umeå University (2014).

[6] S. Gordienko, A. Pukhov, Scalings for ultrarelativistic laser plasmas and quasimonoenergetic electrons, Physics of Plasmas 12 (4) (2005) 043109–043109–11.

[7] J. D. Jackson, Classical electrodynamics, Wiley, New York, 1999.

[8] P. McKenna, S. (e-book collection), Laser-plasma interactions and applications, Springer, New York; Switzerland, 2013.

[9] C. K. Birdsall, A. B. Langdon, Plasma physics via computer simulation, Vol. 71, Taylor and Francis, 2005.

[10] J. e. a. Meyer-ter Vehn, A parallel one-dimensional relativistic electromagnetic particle-in-cell code for simulating laser-plasma-interaction, AIP Conference Proceedings.

A Additional simulations

To ensure that the RES-AP model agreed with the Particle-in-cell simulations for an arbitrarily polarized incident wave the results in Fig. 23 and 22 are included. The simulations performed were of a pulse with $\theta = 12°$, $S_y = 2$, $a_{y,0} = 85$, $a_{z,0} = a_{y,0}/1.5$ and $\Psi = \pi/3$.

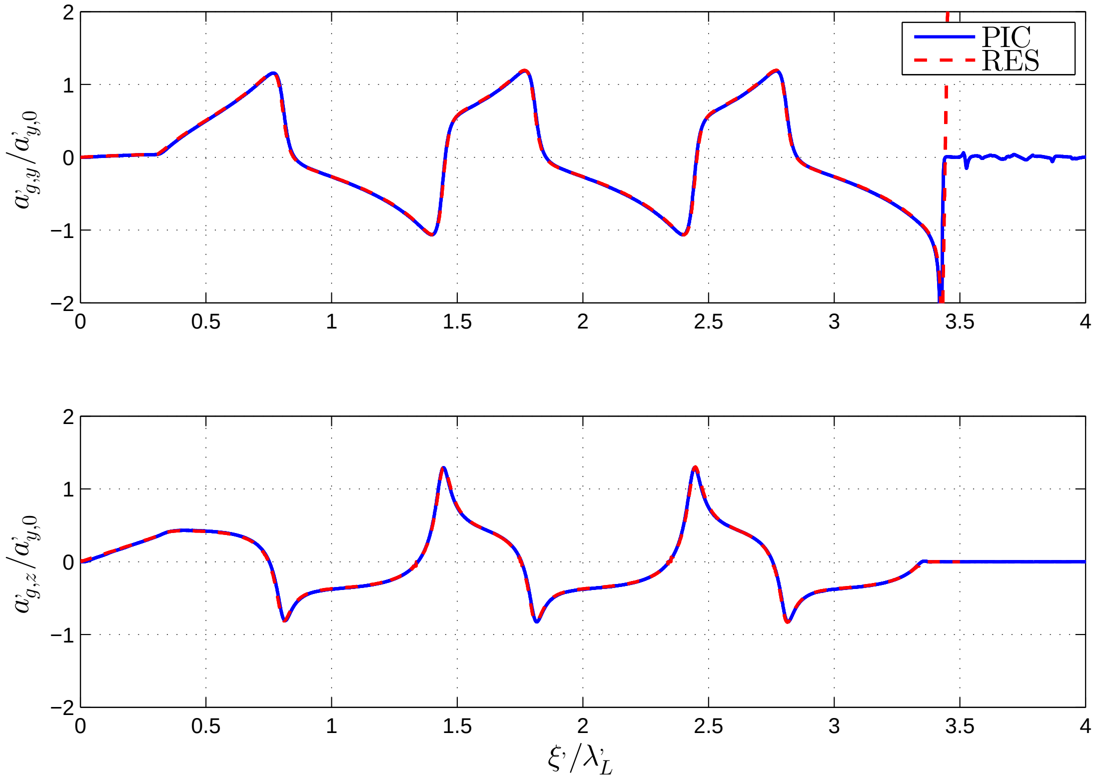

Figure 22: The y- (top) and z-component (bottom) of the electric field obtained from PIC simulations (solid) and the RES-AP model (dashed). The simulation parameters used were $\theta = 12°$, $S = 2$, $a_{y,0} = 85.0$, $a_{z,0} = a_{y,0}/1.5$ (corresponding to $I = 10^{22}$ W/cm^2 for $\lambda = 1\mu$m), plasma thickness $L = 2\lambda'$, $\Delta t = \Delta x = 0.05\omega_p$ for 50 macroparticles per cell. For the RES-AP simulation $\gamma_p = 5$ was used.

Fig. 24 the interaction of the entire circularly polarized pulse is considered when extracting the maximum amplification of the field (as opposed to Fig. 12 where only the homogeneous part of the wave is considered) is shown. An additional area of amplification of the y-component is obtained that is not present in Fig. 12 for $\theta < 20°$. This area in the S,θ-plane would be interesting to investigate further if

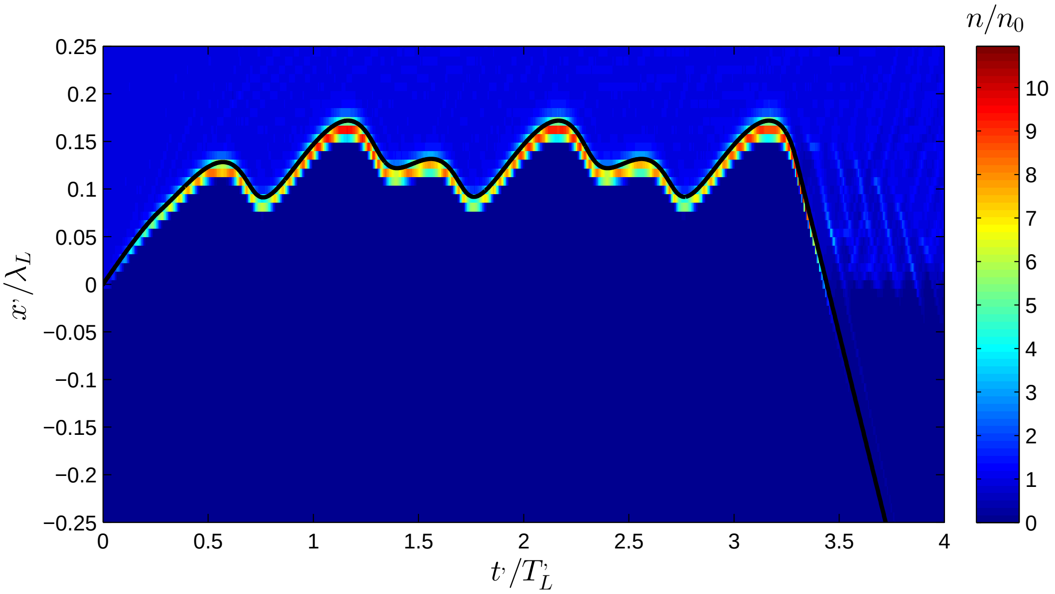

Figure 23: The time evolution of the plasma density obtained from PIC simulations compared with the dynamics of the boundary layer obtained from the RES-AP model (black line). The simulation parameters used were $\theta = 12°$, $S = 2$, $a_{y,0} = 85.0$, $a_{z,0} = a_{y,0}/1.5$ (corresponding to $I = 10^{22}$ W/cm^2 for $\lambda = 1\mu$m), plasma thickness $L = 2\lambda'$, $\Delta t = \Delta x = 0.05\omega_p$ for 50 macroparticles per cell. For the RES-AP simulation $\gamma_p = 5$ was used.

it would be possible to combine a circularly polarized and a p-polarized wave to boost the amplification of the giant pulse even more.

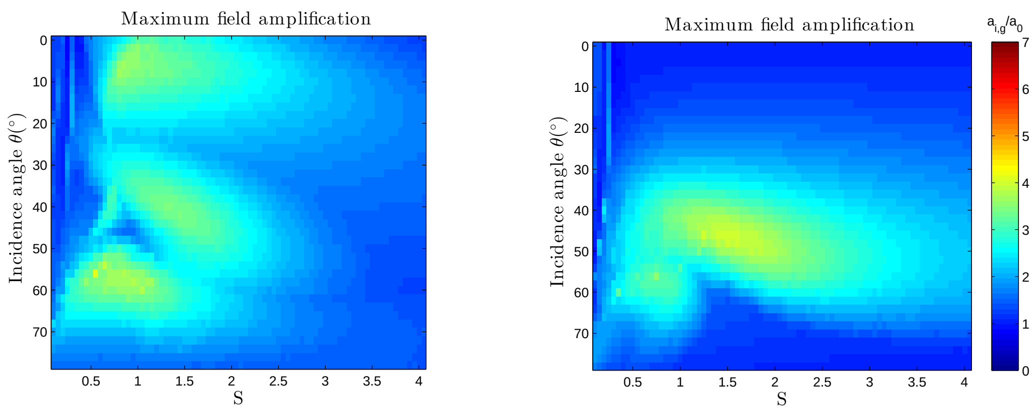

Figure 24: Maximum amplification of y- (left) and z-component (right) of electric field obtained from PIC simulations with varying incident angle θ and similarity parameter S for a right-going circular polarized laser. The simulation parameters used were $a_{y,0} = a_{z,0} = 42.5$ (corresponding to $I = \cdot 10^{22}$ W/cm^2 for $\lambda = 1\mu$m), plasma thickness $L = 4\lambda'$, $\Delta t = \Delta x = 0.1\omega_p$ for 40 macroparticles per cell.